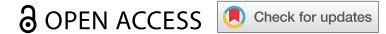Taylor & Francis
Taylor & Francis Group

RESEARCH PAPER

Modulating FKBP5/FKBP51 and autophagy lowers HTT (huntingtin) levels

Barbara J. Bailus[a,b], Stephen M. Scheeler[a,c], Jesse Simons[a], Maria A. Sanchez[a], Kizito-Tshitoko Tshilenge[a], Jordi Creus-Muncunill[d], Swati Naphade[a], Alejandro Lopez-Ramirez[a], Ningzhe Zhang [a], Kuruwitage Lakshika Madushani[a], Stanislav Moroz[a], Ashley Loureiro[a], Katherine H. Schreiber[a], Felix Hausch [e], Brian K. Kennedy[a,f,g], Michelle E. Ehrlich[d], and Lisa M. Ellerby[a]

[a]The Buck Institute for Research on Aging, Novato, CA, USA; [b]School of Pharmacy and Health Sciences, Keck Graduate Institute, Claremont, CA, USA; [c]Leonard Davis School of Gerontology, University of Southern California, Los Angeles, CA, USA; [d]Department of Neurology, Icahn School of Medicine at Mount Sinai, New York, NY, USA; [e]Institute for Organic Chemistry and Biochemistry, Technische Universität Darmstadt, Darmstadt, Germany; [f]Departments of Biochemistry and Physiology, Yong Loo Lin School of Medicine, National University Singapore, Singapore; [g]Centre for Healthy Longevity, National University Health System, Singapore

ABSTRACT

Current disease-modifying therapies for Huntington disease (HD) focus on lowering mutant HTT (huntingtin; mHTT) levels, and the immunosuppressant drug rapamycin is an intriguing therapeutic for aging and neurological disorders. Rapamycin interacts with FKBP1A/FKBP12 and FKBP5/FKBP51, inhibiting the MTORC1 complex and increasing cellular clearance mechanisms. Whether the levels of FKBP (FK506 binding protein) family members are altered in HD models and if these proteins are potential therapeutic targets for HD have not been investigated. Here, we found levels of FKBP5 are significantly reduced in HD R6/2 and zQ175 mouse models and human HD isogenic neural stem cells and medium spiny neurons derived from induced pluripotent stem cells. Moreover, FKBP5 interacts and colocalizes with HTT in the striatum and cortex of zQ175 mice and controls. Importantly, when we decreased FKBP5 levels or activity by genetic or pharmacological approaches, we observed reduced levels of mHTT in our isogenic human HD stem cell model. Decreasing FKBP5 levels by siRNA or pharmacological inhibition increased LC3-II levels and macroautophagic/autophagic flux, suggesting autophagic cellular clearance mechanisms are responsible for mHTT lowering. Unlike rapamycin, the effect of pharmacological inhibition with SAFit2, an inhibitor of FKBP5, is MTOR independent. Further, *in vivo* treatment for 2 weeks with SAFit2, results in reduced HTT levels in both HD R6/2 and zQ175 mouse models. Our studies establish FKBP5 as a protein involved in the pathogenesis of HD and identify FKBP5 as a potential therapeutic target for HD.

Abbreviations: ACTB/β-actin: actin beta; AD: Alzheimer disease; BafA1: bafilomycin A$_1$; BCA: bicinchoninic acid; BBB: blood brain barrier; BSA: bovine serum albumin; CoIP: co-immunoprecipitation; DMSO: dimethyl sulfoxide; DTT: dithiothreitol; FKBPs: FK506 binding proteins; HD: Huntington disease; HTT: huntingtin; iPSC: induced pluripotent stem cells; MAP1LC3/LC3:microtubule associated protein 1 light chain 3; MAPT/tau: microtubule associated protein tau; MES: 2-ethanesulfonic acid; MOPS: 3-(N-morphorlino)propanesulfonic acid); MSN: medium spiny neurons; mHTT: mutant huntingtin; MTOR: mechanistic target of rapamycin kinase; NSC: neural stem cells; ON: overnight; PD: Parkinson disease; PPIase: peptidyl-prolyl *cis/trans*-isomerases; polyQ: polyglutamine; PPP1R1B/DARPP-32: protein phosphatase 1 regulatory inhibitor subunit 1B; PTSD: post-traumatic stress disorder; RT: room temperature; SQSTM1/p62: sequestosome 1; SDS-PAGE: sodium dodecyl sulfate-polyacrylamide gel electrophoresis; TBST:Tris-buffered saline, 0.1% Tween 20; TUBA: tubulin; ULK1: unc-51 like autophagy activating kinase 1; VCL: vinculin; WT: littermate controls.

Introduction

Huntington disease (HD) is a rare, age-associated, autosomal-dominant neurological disease caused by a triplet repeat CAG expansion in exon 1 of the *HTT* (huntingtin) gene (The Huntington's Disease Collaborative Research Group [1]). CAG codes for glutamine and, therefore, the expansion of CAG in the *HTT* gene results in a polyQ (polyglutamine) expanded tract at the N terminus of the HTT protein, which drives disease pathogenesis. HD patients suffer from significant progressive loss of medium spiny and cortical neurons [2,3], which correlates with

a triad of disease symptoms: cognitive decline, chorea and delusions/personality changes [4]. Treatments for HD are limited, and therapeutic strategies to reduce the HTT levels are being pursued in patients [5,6].

FKBPs (FK506 binding proteins) have been studied in relationship to their binding of immunosuppressant drugs FK506 and rapamycin [7–11] and are highly expressed in the central nervous system. As a result of rapamycin binding, FKBPs can regulate the MTOR (mechanistic target of rapamycin kinase) pathway, thus influencing transcriptional and

hormonal regulation, protein folding, and neuronal development [12–21]. The levels and ratios of FKBP family members are important in determining the efficacy and side effects of rapamycin [12], and the ratio of FKBP5/FKBP51 to FKBP4/FKBP52 regulates neurite outgrowth, neuroendocrine feedback, and stress coping behavior in mice [11,16,22–25].

FKBP5 and FKBP4 have been implicated in neurological disorders, including Parkinson disease (PD), Alzheimer disease (AD), post-traumatic stress disorder (PTSD) and schizophrenia [21,26–31]. FKBP4 binds to MAPT/tau (microtubule associated protein tau), regulating its function and degradation, and FKBP5 prevents MAPT degradation and enhances neurotoxicity [27,32]. In PD, FKBP5 contributes to neuronal cell death by acting as a substrate for PTEN induced putative kinase (PINK1) [33]. In PTSD, the glucocorticoid receptor and FKBP5 protein complex is elevated in PTSD patients and disrupting this complex in mice reverses behavioral and molecular changes induced by fear conditioning in mice [34]. FKBP5 is also linked to depression, bipolar disorder, and schizophrenia through this pathway [35]. The role of FKBP1A/FKBP12, another family member, has been studied in detail in neurological diseases. FKBP1A binds and affects the processing of amyloid precursor protein, linking this enzyme to AD pathology, and contributes to alpha-synuclein toxicity via a calcineurin-dependent process. Currently, we do not know the relative contributions and mechanisms for these distinct FKBP family members in neurological diseases.

Functionally, FKBPs are peptidyl-prolyl *cis/trans*-isomerases (PPIases), able to convert prolines in proteins from a cis to a trans configuration. The isomerization activity of FKBP5 increases α-synuclein aggregation [36–38]. HTT protein contains multiple proline-rich regions adjacent and near to the polyQ stretch that could be targets for FKBP activity. The orientation of the proline-rich regions affects the conformation of the HTT protein and subsequent formation of aggregates *in vitro* [39–43]. Given the potential of rapamycin as a therapeutic for HD and the importance of the proline-rich region of HTT on protein conformation, we evaluated the role of FKBPs in HD. In this study, we examined FKBP family members FKBP1A, FKBP1B/FKBP12.6, FKBP5 and FKBP4, in both mice and an isogenic human cellular model of HD [44]. Of note, small molecule inhibitors of FKBP family members have been developed, and one, called SAFit2, is a promising pharmacological agent that inhibits FKBP5 proline isomerase activity and crosses the blood brain barrier (BBB) [16,45]. This small molecule selectively targets FKBP5, but not the closely related FKBP4. Our findings indicate that FKBP levels are altered in HD, modulation of FKBP5 levels or inhibition of FKBP5 could be a therapeutic target for HD by reducing HTT levels.

Results

FKBP5 is decreased in the HD zQ175 knockin mouse model

zQ175 mice are a well-established knockin mouse model of HD with 175 polyQ repeats that exhibit numerous biochemical and neuropathological changes, reflecting HD phenotypes starting at 6 months of age and are robust at 12 months of age [46,47]. The zQ175 model, which expresses full-length HTT protein, is ideal

from the genetic perspective because expression of mutant HTT occurs in the appropriate genetic and protein level. We compared expression changes in FKBP family members in the zQ175 and WT (littermate controls) at 12-months of age, using western blot analysis of proteins from the striatum and cortex (Figure 1A,E). The striatum showed 3.4-fold less FKBP5 expression in zQ175 mice than WT (Figure 1B, **p ≤ 0.01). Expression of FKBP1A and FKBP1B was slightly less in the zQ175 than WT in the striatum, but this did not reach statistical significance (Figure 1C,D). The levels of FKBP5 were slightly lower in the cortex (Figure 1E,F). Levels FKBP1A and FKBP1B in the cortex of zQ175 were essentially the same as in WT (Figure 1E,G,H). Analysis of the published transcriptomics of zQ175 mice compared to WT (RNA-seq) did not show a significant decrease in *FKBP5* mRNA expression levels [48].

FKBP expression is altered in HD R6/2 mice

Next, using western blot analysis, we evaluated the FKBP expression levels in another mouse model of HD. The HD R6/2 mouse model expresses a protein derived from the expanded exon 1 of *HTT* and has accelerated HD phenotypes and pathology, as well as earlier onset of death at 21 weeks in a C57/B6 background [49–53]. We compared expression changes in FKBP family members in the R6/2 and WT mice at 16 weeks of age in the striatum and cortex (Figure 2A,E). At 16 weeks of age, the R6/2 have significant behavioral and neuropathological changes from the expression of the toxic exon 1 derived HTT fragment. The expression of FKBP5 was 2.3-fold lower in the striatum of the R6/2 mice than in WT mice at 16 weeks of age (Figure 2B, *p ≤ 0.05). There were also small but significant decreases in the levels of FKBP1B (Figure 2C, 1.2-fold, **p ≤ 0.01) and FKBP1A (Figure 2D, 1.3-fold, ***p ≤ 0.001) in the R6/2 when compared to WT. In the cortex, there was no statistical difference in any of the FKBP levels (Figure 2E-F). The altered expression levels of FKBPs in the R6/2 were comparable to those observed in the zQ175 model.

Differential expression of FKBPs in HD striatum and cortex

In HD, both the cortex and the striatum are affected, and we compared the relative levels of FKBP5 in the striatum to the cortex. FKBP proteins may affect these two regions of the brain differently. We determined if the level of expression of the FKBP5 differs in the striatum and cortex of the WT and zQ175 mice. Western blot analysis showed FKBP5 is expressed 1.7 times higher in the striatum than the cortex of WT mice (Figure 3A,B, *p ≤ 0.05) at 12 month of age. Similarly, FKBP1B and FKBP1A had higher expression levels in the striatum than the cortex (Figure 3C,D, **p ≤ 0.01). The difference in enrichment of FKBPs in the striatum was lost in the zQ175 mice, consistent with the lower levels of FKBP5 observed in this HD model (Figure 3F-H).

FKBP5 levels are decreased in zQ175 mice at 6 months of age

To determine when FKBP5 levels change during disease progression, we measured the levels in WT and zQ175 mice at 6 and 12 months of age. At 6 months of age,
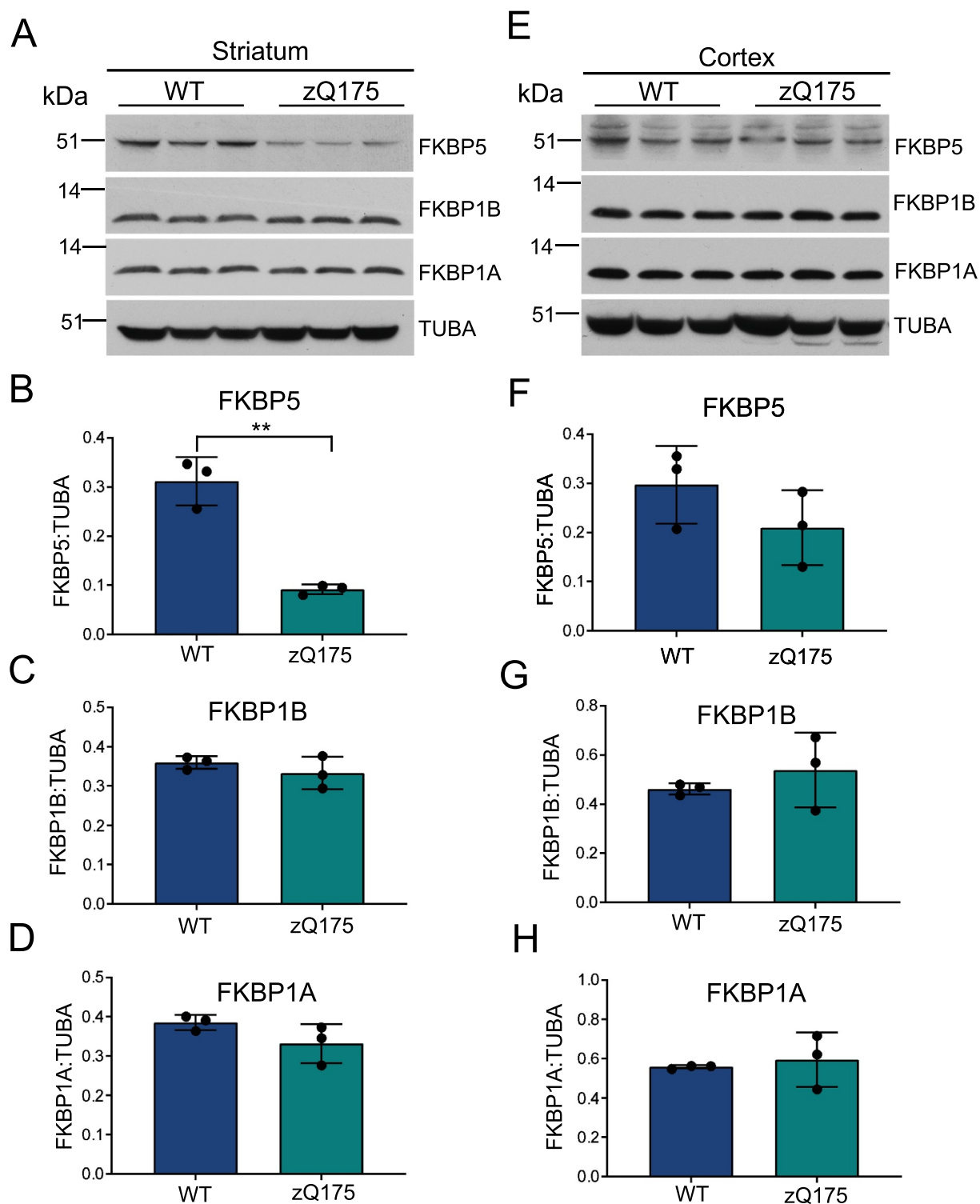
Figure 1. FKBP expression levels in HD zQ175 mouse model. (A) representative western blots analysis of FKBP5, FKBP1B and FKBP1A in WT and zQ175 homozygote mouse striatum at 12 months of age. (B-D) Quantification of the expression levels of FKBP5 (B), FKBP1B (C), and FKBP1A (D) in the striatum normalized to TUBA/α-tubulin. statistically significant difference in FKBP expression is indicated (t-test, **p ≤ 0.01). (E) Representative western blots of FKBP5, FKBP1B and FKBP1A in WT, compared to zQ175 homozygote mouse cortex at 12 months of age. (F-H) Quantification of the expression levels of FKBP5 (F), FKBP1B (G), and FKBP1A (H) in the cortex normalized to TUBA. No statistically significant difference was observed between WT and zQ175 cortex FKBPs expression levels (t-test).

measurable changes in mHTT aggregates, metabolites, brain atrophy and biochemical changes were detected [46,47]. WT mice showed no change in FKBP5 striatal levels from 6 to 12 months (Figure 4A,B). There was a decrease in the FKBP5 levels in the striatum of zQ175

mice at 6 (*p ≤ 0.05) and 12 months of age (**p ≤ 0.01), compared to WT mice (Figure 4A,B, ***p ≤ 0.001). There was an age-dependent decrease in FKBP5 levels in zQ175 mice at 6 and 12 months of age. The difference between the zQ175 and WT FKBP5 levels in the striatum was
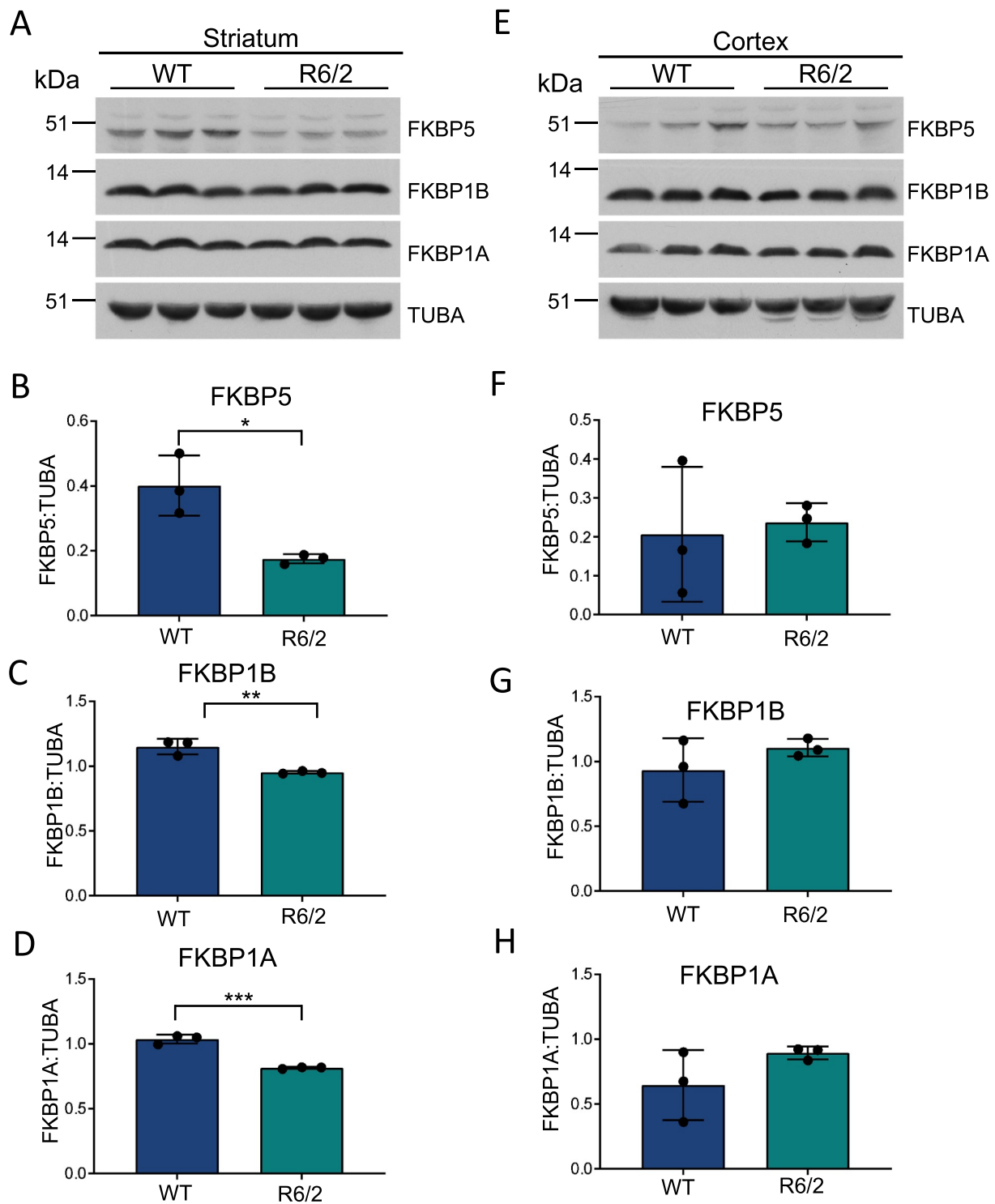
Figure 2. FKBP expression levels in HD R6/2 mouse model. (A) representative western blot analysis of FKBP5, FKBP1B and FKBP1A in WT and R6/2 mouse striatum at 4 months of age. (B-D) Quantification of the expression levels of FKBP5 (B), FKBP1B (C), and FKBP1A (D) in the striatum normalized to TUBA. Statistically significant difference in FKBP expression is indicated (t-test, *p ≤ 0.05, **p ≤ 0.01, ***p ≤ 0.001). (E) Representative western blots of FKBP5, FKBP1B and FKBP1A in WT compared to R6/2 mouse cortex at 4 months of age. (F-H) Quantification of the expression levels of FKBP5 (F), FKBP1B (G), and FKBP1A (H) in the cortex normalized to TUBA. No statistically significant difference was observed between WT and R6/2 cortex FKBPs expression levels (t-test).

statistically significant (***p ≤ 0.001) (Figure 4A,B). There was a significant decrease in the levels of FKBP5 in the cortex of zQ175 mice at 6 and 12 months of age (Figure 4C,D, *p ≤ 0.05). FKBP5 levels in the striatum and cortex decreased during HD disease progression. The effect was more pronounced in the striatum. As expected, the levels of soluble mHTT (defined as resolving on SDS page gel at HTT molecular mass) are decreased during this time
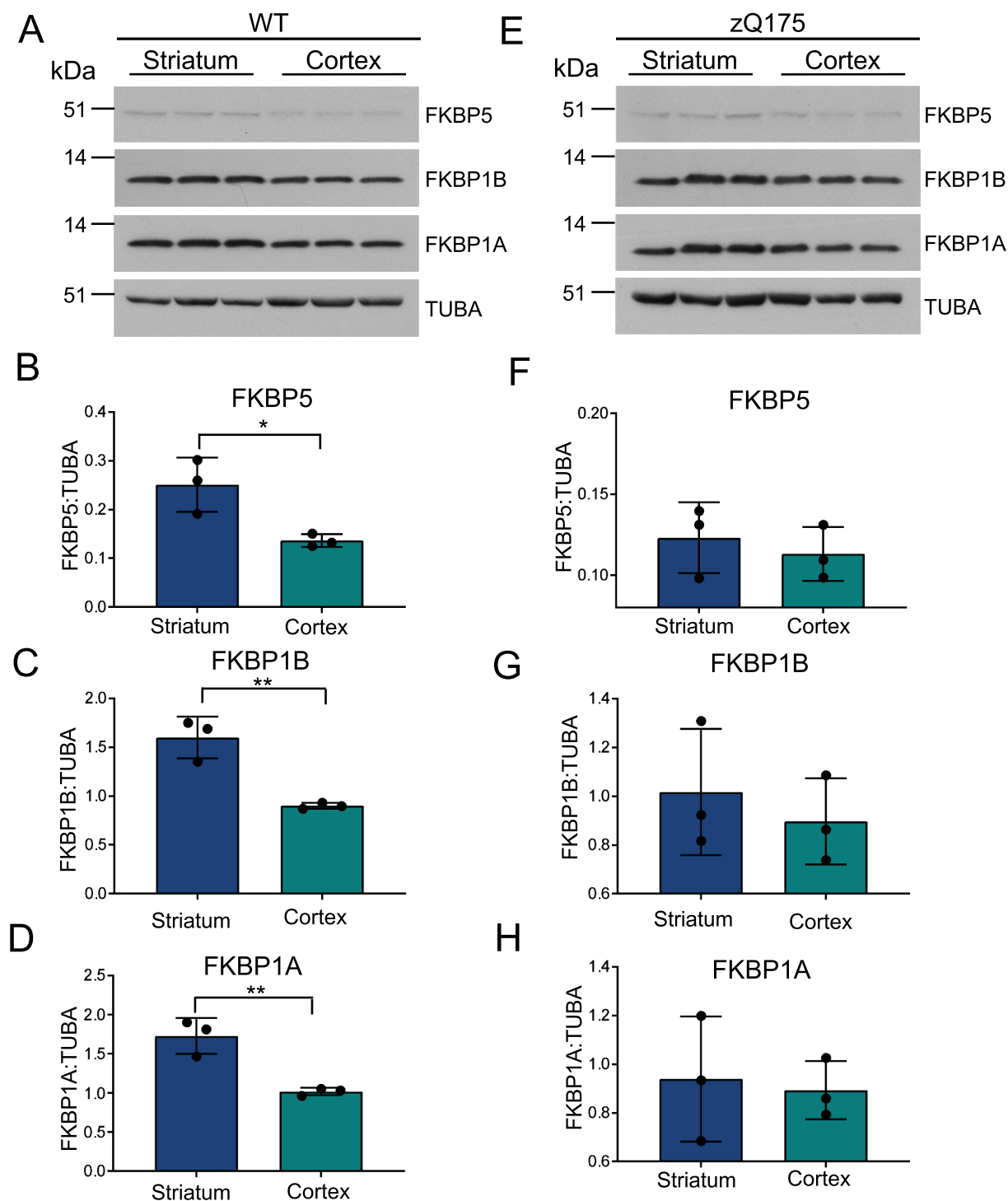
Figure 3. Expression levels of FKBPs in cortex versus striatum in wild-type and zQ175 mice. (A) Representative western blot analysis of FKBP5, FKBP1B and FKBP1A in the striatum and cortex of 12-month-old WT mice. (B-D) Quantification of the expression levels of FKBP5 (B), FKBP1B (C), and FKBP1A (D) in the striatum and cortex normalized to TUBA. statistically significant difference in FKBP expression is indicated (t-test, *p ≤ 0.05, **p ≤ 0.01). (E) Representative western blots of FKBP5, FKBP1B and FKBP1A in the striatum and cortex of 12-month-old homozygote zQ175 mice. (F-H) Quantification of the expression levels of FKBP5 (F), FKBP1B (G), and FKBP1A (H) in the striatum and cortex normalized to TUBA. No statistically significant difference was observed in FKBPs expression levels between striatum and cortex of zQ175 mice (t-test).

frame as measured by antibody to the polyQ stretch (1C2), consistent with previous studies [54,55]. The changes in mHTT may directly correlate with the lower FKBP5 levels (**Figure S1**) and the physical interaction between the proteins described below.

HTT and FKBP5 Co-Immunoprecipitated in Knockin Mouse Models of HD with Increasing PolyQ Repeat Length

A possible mechanism for the lower levels of FKBP5 in the HD mouse models is a physical interaction of FKBP5 with mHTT and
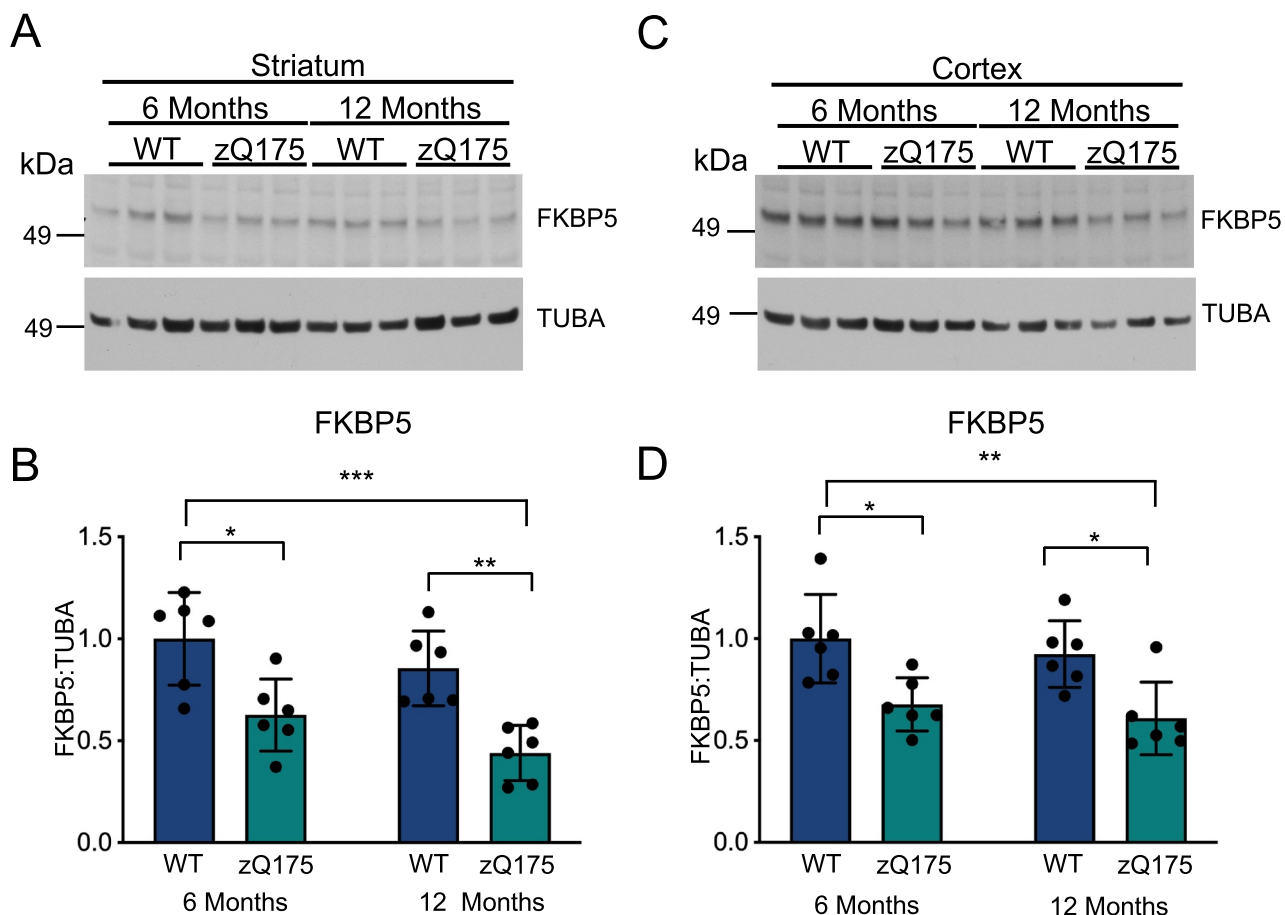
Figure 4. Temporal changes in FKBP5 levels in zQ175 mice. (A,C) representative western blots analysis of striatum (A) and cortex (C) for FKBP5 expression in 6- and 12-month-old mice when compared to homozygote zQ175 to WT. (B,D) Graphs show quantification of the expression levels of FKBP5 when normalized to TUBA. A significant decrease of FKBP5 expression is observed for the striatum (B) and cortex (D) when comparing 12-month-old zQ175 to WT. statistical analysis used ordinary two-way ANOVA (*$p \leq 0.05$; **$p \leq 0.01$; ***$p \leq 0.001$).

the sequestration of FKBP5 into aggregates or insoluble proteins. To determine if FKBP5 interacts with HTT, we used co-immunoprecipitation (CoIP) of lysates from the striatum and cortex of HD knockin mice with increasing CAG repeat lengths: WT, Q50, Q92, and Q175 at 12 months of age [48]. We found that FKBP5 and HTT co-immunoprecipitated with an anti-HTT antibody in striatal and cortical lysates, but not the IgG (negative control) (Figure 5A). The interaction of FKBP5 and HTT was observed in the WT, Q50, Q92, and Q175 indicating that the expanded polyQ lengths did not affect the extent of this interaction. We also examined CoIPs in the midbrain of a 12-month-old zQ175 homozygote because the midbrain had equal levels of FKBP5 expression in WT and zQ175 mice. We observed that mHTT co-immunoprecipitated with FKBP5 with the α-FKBP5 antibody (**Figure S2**) but with some background nonspecific binding. This may be due to the FKBP5 antibody epitope (synthetic peptide corresponding to residues surrounding Arg222 of FKBP5) that may obscure part of an interaction domain with HTT. The results overall indicate that there is a direct or indirect interaction between FKBP5 and HTT. To determine if HTT and FKBP5 colocalized, we used immunohistochemistry to examine zQ175 and WT mice at 12 months of age. Expression of FKBP5 was detected in the cortex and striatum of HD and WT mice. By confocal microscopy, HTT colocalized with FKBP5 (Figure 5B).

HTT colocalized with FKBP5 (20–40%) in the cortex and striatum, and co-localization levels were lower in the zQ175 mice, when compared to WT (Figure 5C).

HD neural stem cells have altered expression of FKBP5

To determine if FKBP5 levels were changed in cellular models of HD we used our human induced pluripotent stem cells (iPSC)-derived isogenic model of HD to determine if this model mirrored some of the expression observed changes in HD mouse models. We performed western blot analysis on the HD and C116 neural stem cells (NSC). We found that the HD NSC had lower levels of FKBP5 than C116 NSC (Figure 6A,B, ****$p \leq 0.0001$). FKBP1A and FKBP1B levels were not altered (Figure 6A,C,D). Using immunocytochemistry, we detected co-localization of FKBP5 and HTT (Figure 6E, **Figure S3**). We observed a decrease in FKBP5 levels in the HD NSC and altered localization of HTT and FKBP5 in the HD NSC, with more FKBP5 localized in the nucleus of the HD NSC than in C116 NSC. We previously generated a transcriptomic profile of human isogenic HD vs. corrected (C116) NSC lines [44,56,57]. The RNA-seq data set of the corrected C116 and HD NSC showed that several FKBPs had a significant decrease in RNA expression levels (**Figure S4**). Accounting for false discovery
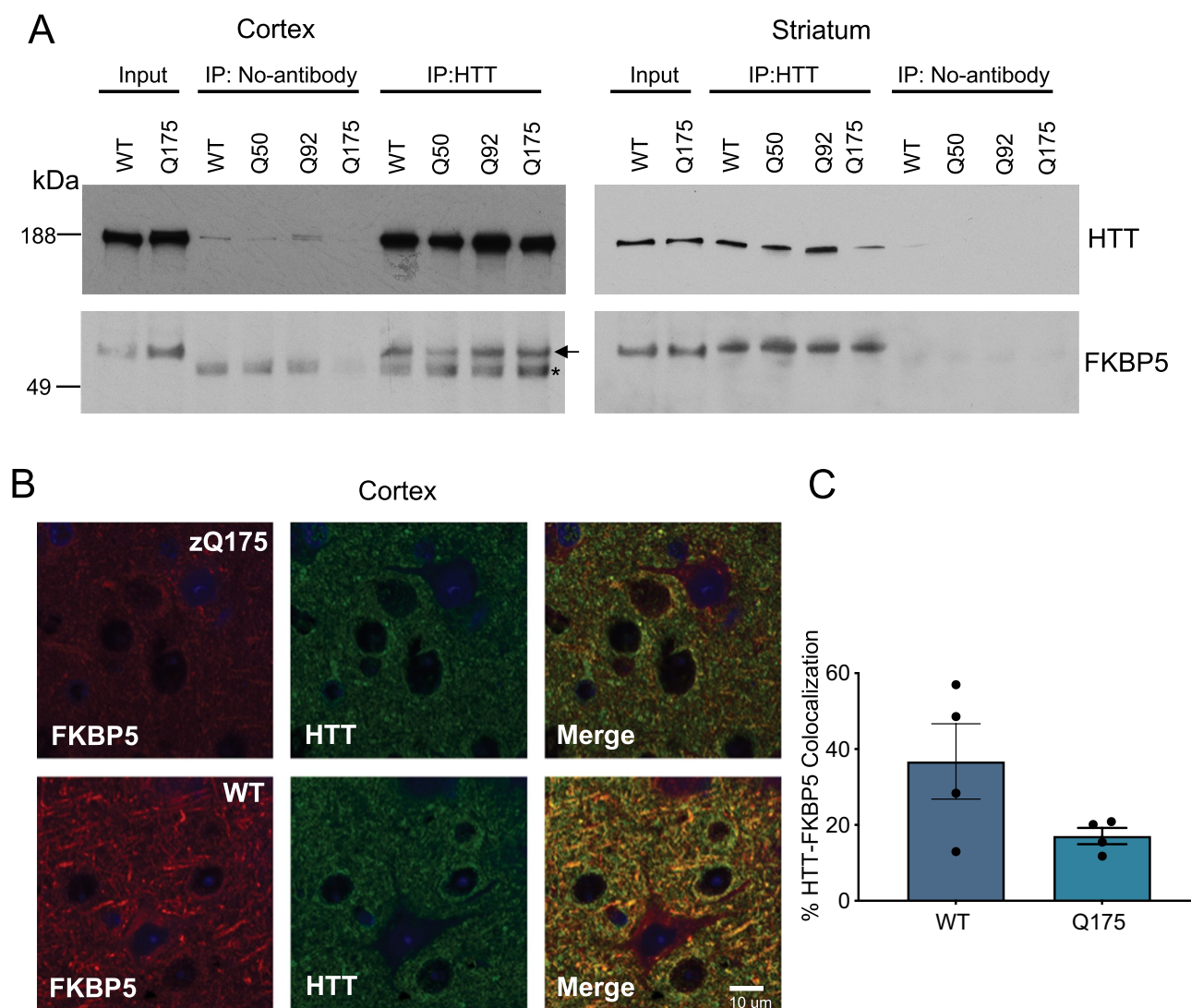
Figure 5. FKBP5 interaction and colocalization with HTT. (A) Cortex and striatal co-immunoprecipitation using α-HTT antibody (Millipore, MAB2166) and probing for FKBP5 in heterozygous allelic HTT mice with increasing polyQ-repeat length. the arrow in the lower left panel indicates the pull down of FKBP5, and the * is IgG protein from the IP. We used heterozygous mice as this was the tissue we had available. additionally, the presence of both WT HTT and mHTT makes this a reasonable comparison. (B) Confocal analysis of HTT (green) and FKBP5 (red) demonstrates the colocalization of FKBP5 and HTT in the cortex in both WT and homozygous zQ175 mice. (C) Quantification of the percentage of HTT colocalizing with FKBP5 (right panel).

rate, FKBP1B and FKBP5 were expressed at lower levels in the HD NSC than C116 NSC (p = 8.98E-18 and p = 0.0002, respectively). As described above, the HD mouse models do not have alterations in the FKBP5 levels at the transcriptional level. Therefore, cell-specific effects not detected in mouse tissue will warrant further analysis.

FKBP5 expression levels are decreased in HD medium spiny neurons

One of the main cell types lost in HD is medium spiny neurons (MSN). Therefore, we differentiated our isogenic HD and C116 NSC into MSN to evaluate the impact of mHTT on FKBP5 levels in this highly relevant human cell type (Figure 7A). HD and C116 MSN express high levels of PPP1R1B/DARPP-32 (protein phosphatase 1 regulatory inhibitor subunit 1B), one of markers of MSN (Figure 7B). As expected, the levels of

PPP1R1B are lower in the HD MSN than the C116 MSN as this is a known signature of HD pathogenesis (Figure 7B). We found the endogenous levels of FKBP5 in HD MSN were significantly lower than in C116 MSN (Figure 7C,D, **p ≤ 0.01).

siRNA knockdown of FKBP5 in HD neural stem cells reduces mHTT levels

Transcriptomic and proteomic expression analyses in HD suggest that dysregulated expression reflects compensatory, non-pathogenic, and disease-driving responses due to the polyQ expansion in HD [58]. A critical target in the cellular response to HD is the expression of the toxic mHTT protein. FKBP5 prevents degradation of MAPT and contributes to its aggregation and toxicity [32,59]. Therefore, we decided to investigate the effect of lowering FKBP5 or blocking FKBP5 isomerase activity on mHTT levels. We treated our isogenic HD and corrected
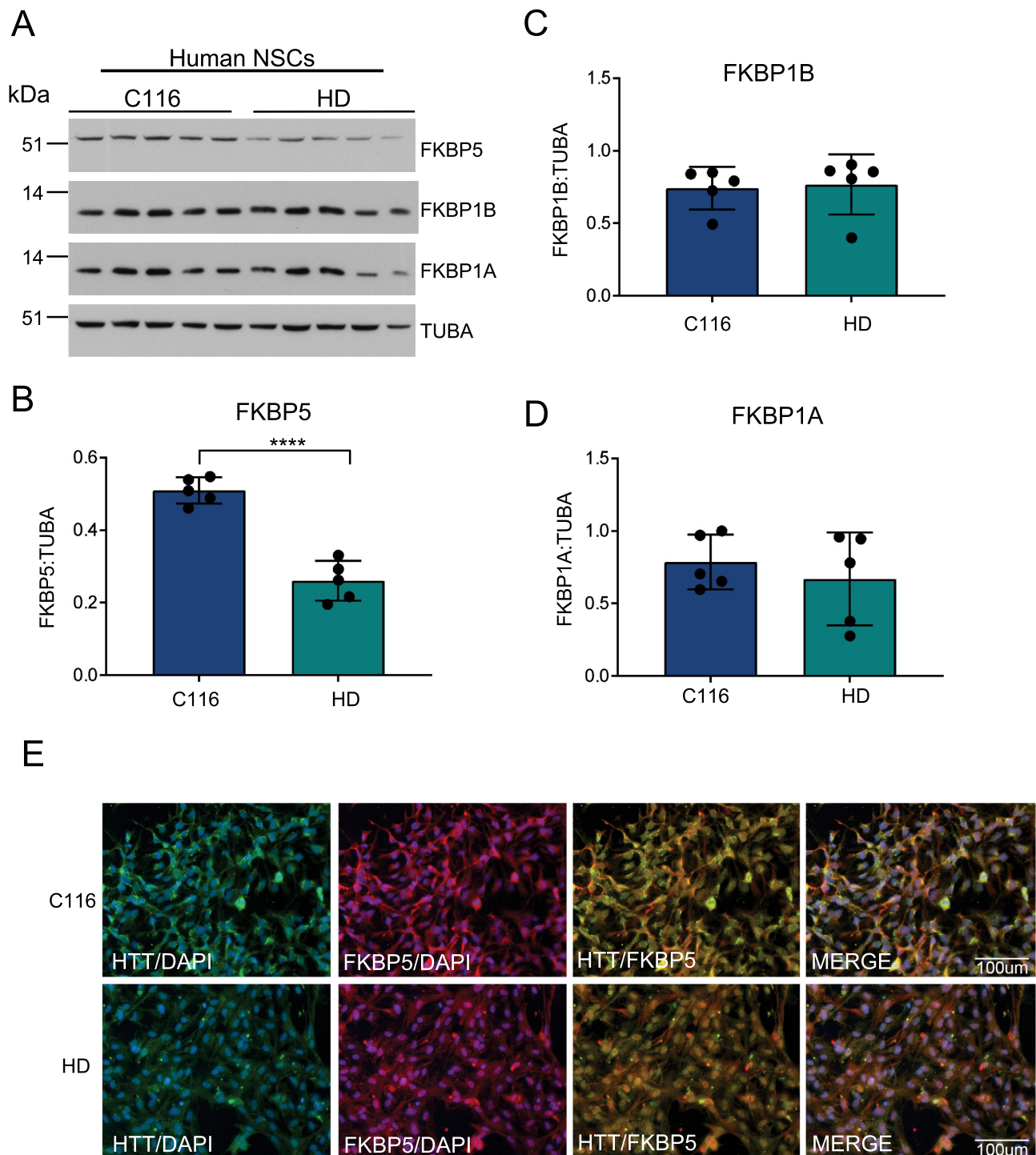
Figure 6. FKBP5 expression and localization in human neural stem cell model. (A) Representative western blots analysis of FKBP5, FKBP1B and FKBP1A in HD and corrected (C116) NSC. (B-D) Quantification of the expression levels of FKBP5 (B), FKBP1B (C), and FKBP1A (D) in NSC normalized to TUBA. A statistically significant difference in FKBP expression is indicated (t-test, ****$p \leq 0.0001$). (E) Immunocytochemistry of HD and C116 NSC stained with FKBP5 (red) and HTT (green) antibodies.

C116 NSC lines with siRNA to FKBP5. We observed a significant knockdown of FKBP5, approximately 20% in both HD and C116 NSC, when compared to the non-targeting siRNA (**$p < 0.01$, Figure 8A,B). The knockdown in HD NSC produced a significant decrease in mHTT levels compared to the control siRNA when normalized to ACTB/β-actin (actin beta) (*$p \leq 0.05$, Figure 8C). This decrease in mHTT levels mediated

by siRNA-enforced reduction in FKBP5 suggests that modulation of this enzyme is a therapeutic strategy for HD.

SAFit2 treatment of HD neural stem cells

FKBP5 and FKBP4 have been extensively studied for their roles in neurite retraction and extension, as well as in stress
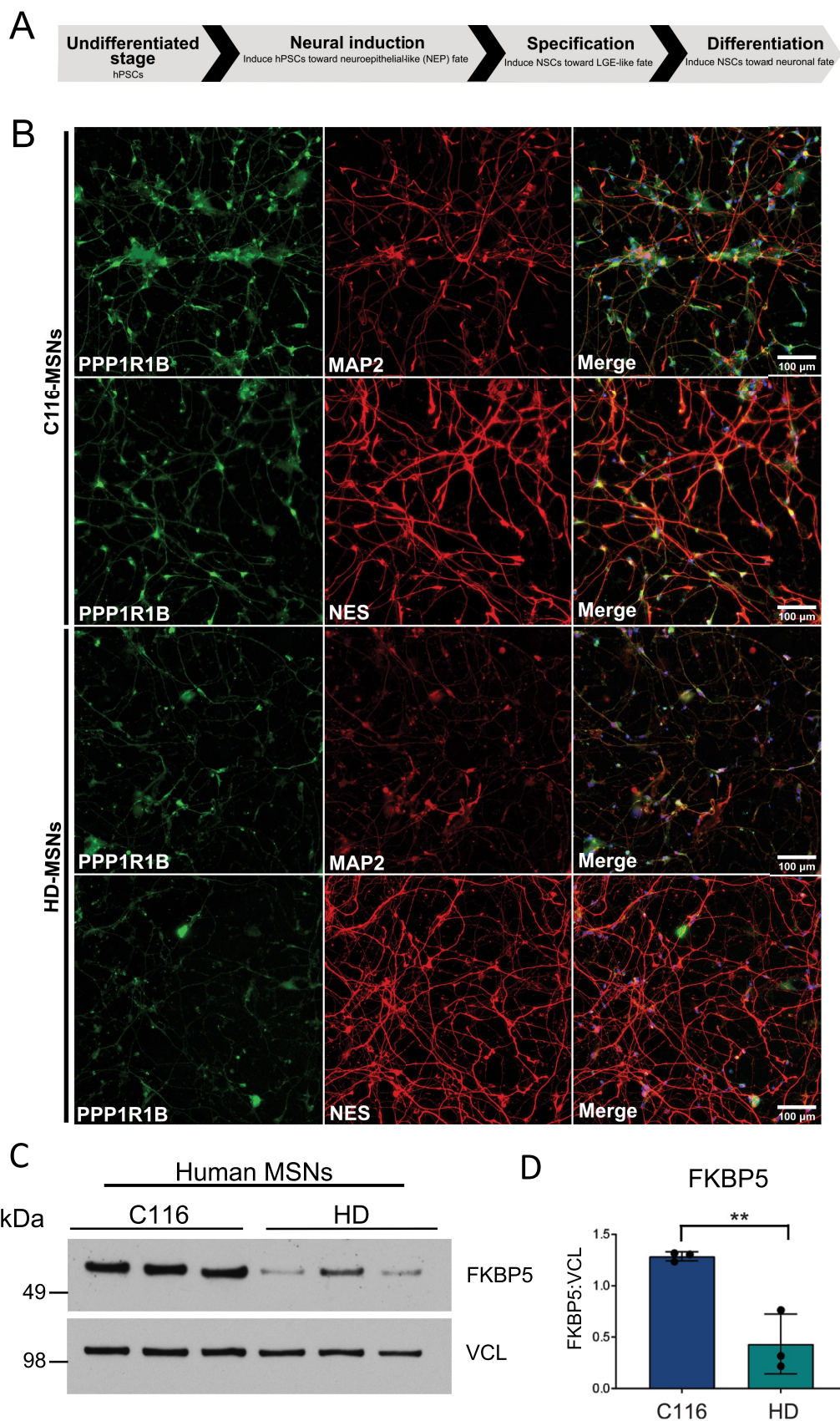
Figure 7. FKBP5 levels in human medium spiny neurons derived from patient HD induced pluripotent stem cells. (A) Graphical illustration of MSN differentiation protocol. (B) Human C116 and HD MSN model express PPP1R1B/DARPP-32 (green), MAP2 (red) and NES (nestin; red). (C) Expression levels of FKBP5 in HD and C116 human MSN as measured by western blot analysis. (D) Quantification of expression levels of FKBP5 normalized to VCL (vinculin) are shown (**p ≤ 0.01, t-test).

Figure 8. Evaluation of HTT levels with genetic or pharmacological inhibition of FKBP5 in neural stem cells. (A) A representative western blot analysis showing the decrease in FKBP5 and HTT levels when treated with FKBP5 siRNA, compared to non-targeting siRNA (NT) and normalized to ACTB. POLYQ antibody 1C2 (Millipore, MAB1574) was used to quantify mHTT levels. (B) Quantification of levels of FKBP5 show a statistically significant decrease in FKBP5 levels upon treatment with FKBP5 siRNA in both genotypes (HD and C116). statistical anal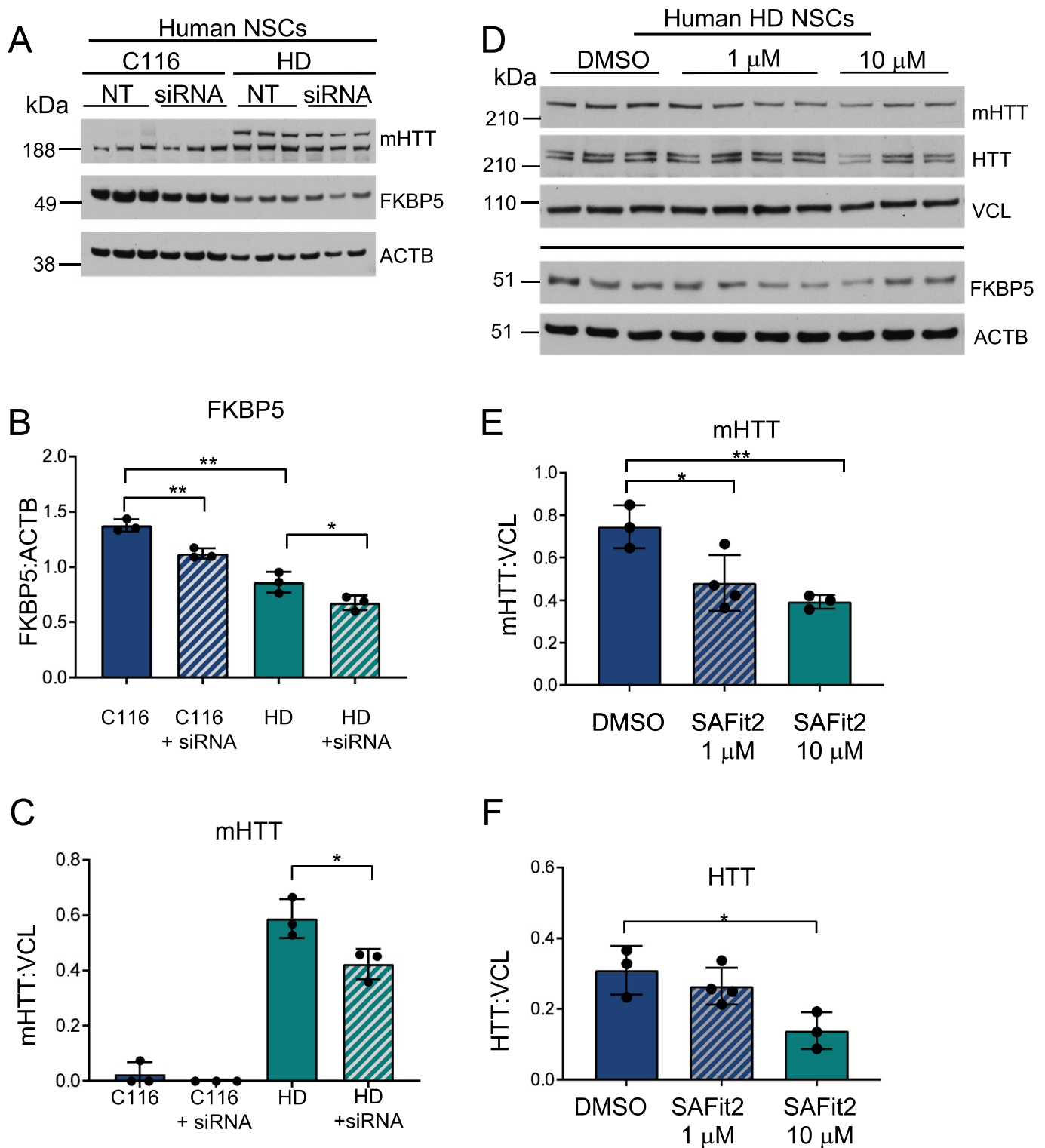ysis used ordinary one-way ANOVA and t-test (*$p \leq 0.05$, **$p \leq 0.01$). (C) The levels of mHTT are significantly (t-test, *$p \leq 0.05$) lower (30%) in the siRNA-treated HD cells. (D) Representative western blot analysis of treatment of HD NSC with SAFit2 at 1 and 10 µM probing with HTT and FKBP5 antibodies. HTT antibody (Millipore, MAB2166) was utilized to measure WT and mHTT levels separating the WT and mHTT on 3–8% Tris-acetate gels. PolyQ antibody 1C2 (Millipore, MAB1574) was used to detect only mHTT levels. (E) Quantification of mHTT levels at both 1 µM and 10 µM, when compared to control (*$p \leq 0.05$, **$p \leq 0.01$). (F) Quantification of normal HTT levels at 1 µM and 10 µM SAFit2 when compared to control. Statistical analysis used ordinary one-way ANOVA and t-test (*$p \leq 0.05$).
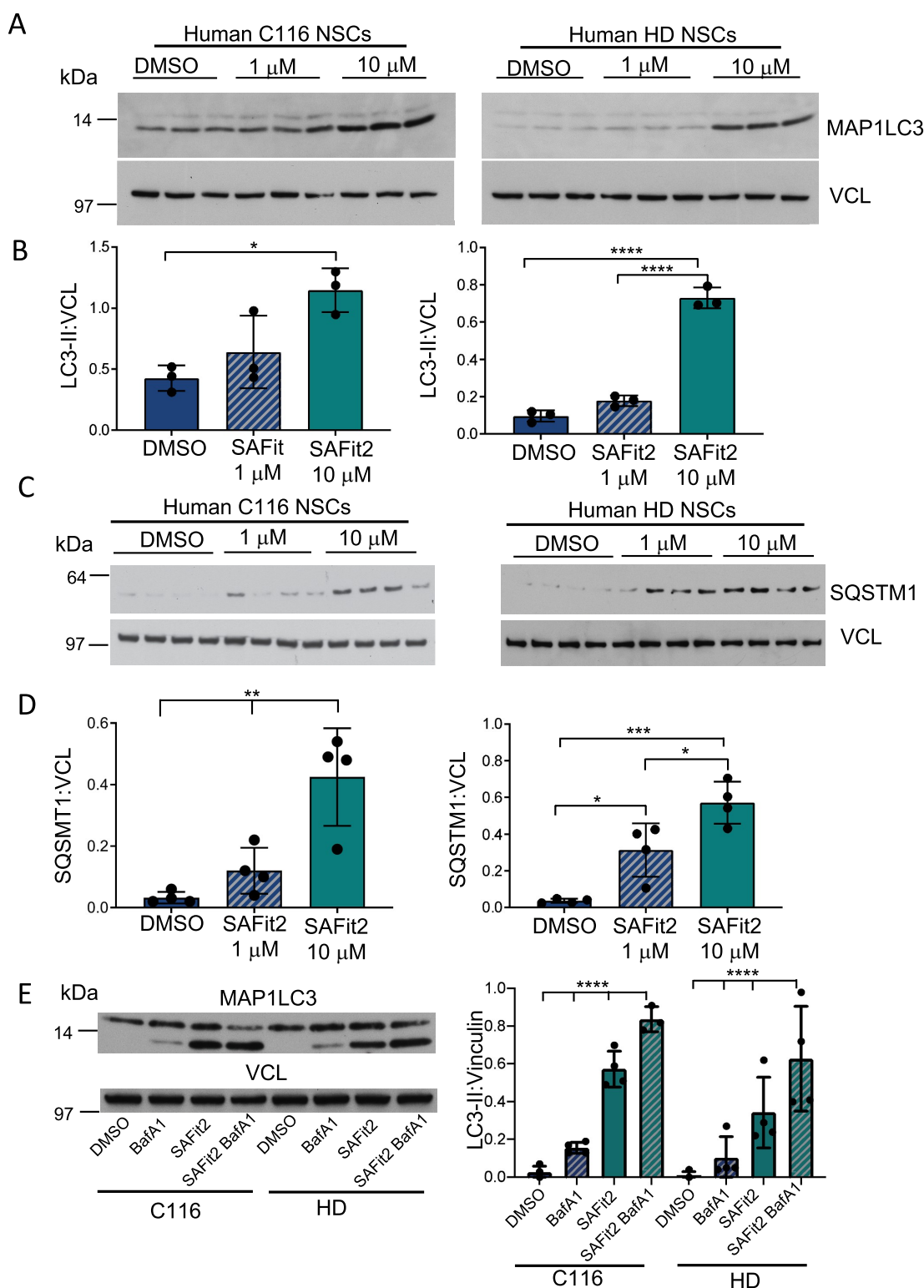
Figure 9. Changes in the expression of LC3 and SQSTM1/p62 with SAFiT2 treatment in HD neural stem cells. (A) A representative western blot analysis showing LC3 and VCL expression after treatment of C116 and HD NSC with SAFit2 at 1 or 10 μM or vehicle (DMSO). (B) C116 NSC treated with 10 μM SAFit2 show increased expression of LC3 (one-way ANOVA, *p = 0.013), compared to vehicle treated cells. In HD NSC, LC3 expression is increased in cells treated with was 10 μM SAFiT2 (one-way ANOVA, ****p ≤ 0.0001), compared to vehicle treated cells. LC3 expression was normalized to VCL expression. 1 μM SAFiT2 compared to 10 μM SAFiT2 was statistically significant (one-way ANOVA, ****p ≤ 0.0001). (C) A representative western blot analysis showing increase expression of SQSTM1 and VCL in C116 and HD after treatment with SAFit2 or DMSO. (D) C116 NSC treated with 10 μM SAFiT2 show a significant increase in SQSTM1 (one-way ANOVA, **p ≤ 0.01) expression, compared to DMSO-treated cells. A significant difference in SQSTM1 expression is also observed between C116 cells treated with 1 vs 10 μM of SAFit2 (one-way ANOVA, **p ≤ 0.01). In HD NSC, expression of SQSTM1 was increased in cells treated with 1 μM (one-way ANOVA, *p ≤ 0.05) and 10 μM SAFit2 (***p ≤ 0.001), compared to DMSO treated cells. A significant difference in SQSTM1 expression is also observed between HD cells treated with 1 or 10 μM of SAFit2 (one-way ANOVA, *p ≤ 0.05). SQSTM1 levels were normalized to VCL expression. (E) C116 and HD NSC were treated with DMSO, Bafilomycin A1 (BafA1), SAFit2, or SAFit2, followed by BafA1. Western blot analysis normalized to VCL shows increased levels of LC3-II after BafA1 (****p ≤ 0.001), SAFit2 (****p ≤ 0.001) and SAFit2 and BafA1 (****p ≤ 0.001) in both C116 and HD NSC.

responses in the central nervous system. SAFit2 is a promising pharmacological agent that inhibits FKBP5 and modulates stress responses [16,45]. This small molecule selectively targets FKBP5, but not the closely related FKBP4. SAFit2 will inhibit proline isomerize activity of FKBP5 and therefore its enzymatic activity may be required for HTT clearance. To determine if pharmacological inhibition of FKBP5 lowers HTT levels, we tested SAFit2 in HD and C116 NSC. Treatment of NSC with SAFit2 showed a significant reduction in mHTT levels (*p = 0.03) at 1 and 10 μM (Figure 8D,E). SAFit2 also lowered the WT HTT levels but reached statistical significance only at a higher dose of 10 μM (Figure 8F).

SAFit2 treatment of HD neural stem cells alters LC3-II and SQSTM1/p62 levels

Misfolded polyQ-expanded proteins are often cleared through autophagy or by the proteasome. To investigate the mechanism of clearance mediated by SAFit2, we evaluated the levels of MAP1LC3/LC3 (microtubule associated protein 1 light chain 3), a marker of autophagosomes. We found a significant increase in LC3-I and LC3-II (LC3–PE) levels in C116 and HD NSC treated with 10 μM of SAFit2 (*p ≤ 0.05; ****p ≤ 0.0001, respectively) (Figure 9A,B, LC3-II shown in panel B). We also evaluated whether pharmacological inhibition of FKBP5 altered the levels of SQSTM1/p62, another autophagy marker. Levels of SQSTM1/p62 (sequestosome 1) were increased upon treatment with SAFit2 (Figure 9C,D). SQSTM1, which is correlated with ubiquitinated proteins destined for autophagic degradation, is decreased, or increased in expression depending upon the drug or cellular stimulation that leads to autophagy [60–62]. To test the impact of FKBP5 inhibition on autophagic flux, we treated C116 and HD NSC with SAFit2 for 48 h, followed by treatment with bafilomycin A₁ (BafA1) for 4 h. BafA1 is a V-ATPase inhibitor that blocks autophagic flux by preventing the acidification of endosomes and autophagosome-lysosome fusion, leading to the accumulation of LC3-II in normal cells under autophagic-inducing conditions (Figure 9). We found that BafA1 treatment alone increased the levels as expected (Figure 9E). SAFit2 also led to a significant increase in basal LC3-II. When BafA1 treatment was applied, LC3-II levels were increased with the greater BafA1-dependent increase in LC3-II, observed in SAFit2 treated cells, as expected (Figure 9E, Figure S5). This result confirms that SAFit2 increases autophagy flux.

Comparing Rapamycin and SAFit2 molecular mechanisms in HD neural stem cells

Rapamycin enhances health span and is protective in cellular and in vivo models of HD [63,64]. Rapamycin inhibits mTOR, which triggers autophagy and is neuroprotective in HD [65,66]. We compared the impact of rapamycin or SAFit2 on neurotoxicity by treating isogenic HD NSC during serum withdrawal with these compounds (Figure 10A). Both rapamycin and SAFit2 reduced the level of activated caspase enzymatic activity in HD NSC 48 h after serum withdrawal (Figure 10A, left panel). Correspondingly, a dose response suggested both SAFit2 and rapamycin (1, 1.5, 2.0 uM) lowered the levels of activated CASP3 (caspase 3) and CASP7 overall (Figure 10A, right panel). To determine if the SAFit2 mechanism of autophagy activation overlapped with rapamycin, we evaluated MTOR inhibition. We found that rapamycin, but not SAFit2, resulted in the inhibition of the phosphorylation for RPS6/S6, a substrate for MTOR (Figure 10B). Further, rapamycin, but not SAFit2, resulted in a decrease in the phosphorylation of MTOR (Figure 10C). Autophagy induction is controlled by the serine/threonine kinase, ULK1 (unc-51 like autophagy activating kinase 1). We found that SAFit2 increased the levels of phosphorylated ULK1 while rapamycin slightly lowered the level of pULK1 (Figure 10D). Our results suggest that rapamycin and SAFit2 are both neuroprotective, but the mechanisms of autophagy induction are distinct. SAFit2 induction is MTOR independent under normal growth conditions.

SAFit2 treatment in R6/2 and zQ175 mice lowers HTT levels

Current therapeutic treatments for HD focus on lowering HTT levels. Therefore, we evaluated whether SAFit2, which crosses the BBB, could lower HTT levels in mouse models of HD. We injected R6/2 mice with SAFit2 (7.5 mg/kg) intraperitoneally for 7 days and analyzed the expression levels of the HTT exon 1 fragment in the striatum. We found that SAFit2 treatment lowered the levels of the polyQ-expanded fragment in R6/2, compared to vehicle-treated R6/2 mice with a possible shift in migration of the fragment with treatment (Figure 11A,B). The insoluble HTT protein was not decreased at this dose of SAFit2 (Figure 11A,B). However, increasing the doses of SAFit2 to 10 and 15 mg/kg reduced the levels of both the soluble and insoluble HTT protein (**Figure S6**). We also evaluated the effect of SAFit2 treatment in the zQ175 mouse model by treating them at 4 months for 2 weeks with SAFit2 at 15 mg/kg a time point when HD pathogenesis is mild and the HTT protein relatively soluble. We found SAFit2 treatment in the zQ175 also lowered the levels of HTT by ~20% as measured using multiple to HTT antibodies in the striatum (Figure 11C-E).

Discussion

Our studies identified FKBP5 as a novel therapeutic target for HD. FKBP5 levels are reduced in multiple mouse models of HD (i.e., R6/2 and zQ175). The changes in expression in the brain are regional and temporally specific, and the strongest effect on expression was in the striatum. The decrease in FKBP5 can be detected at 6 months of age and is further decreased at 12 months of age in zQ175 mice. The change in levels of FKBP5 may correlate with the decrease in soluble mHTT, which is observed in both our cellular and mouse models of HD. FKBP5 prevents degradation of MAPT and contributes to its aggregation and toxicity [32,59]. Interestingly, we found further lowering the levels of FKBP5 by siRNA or pharmacological inhibition decreases the levels of mHTT. We found that inhibiting FKBP5 in human cellular models of HD and in multiple mouse models
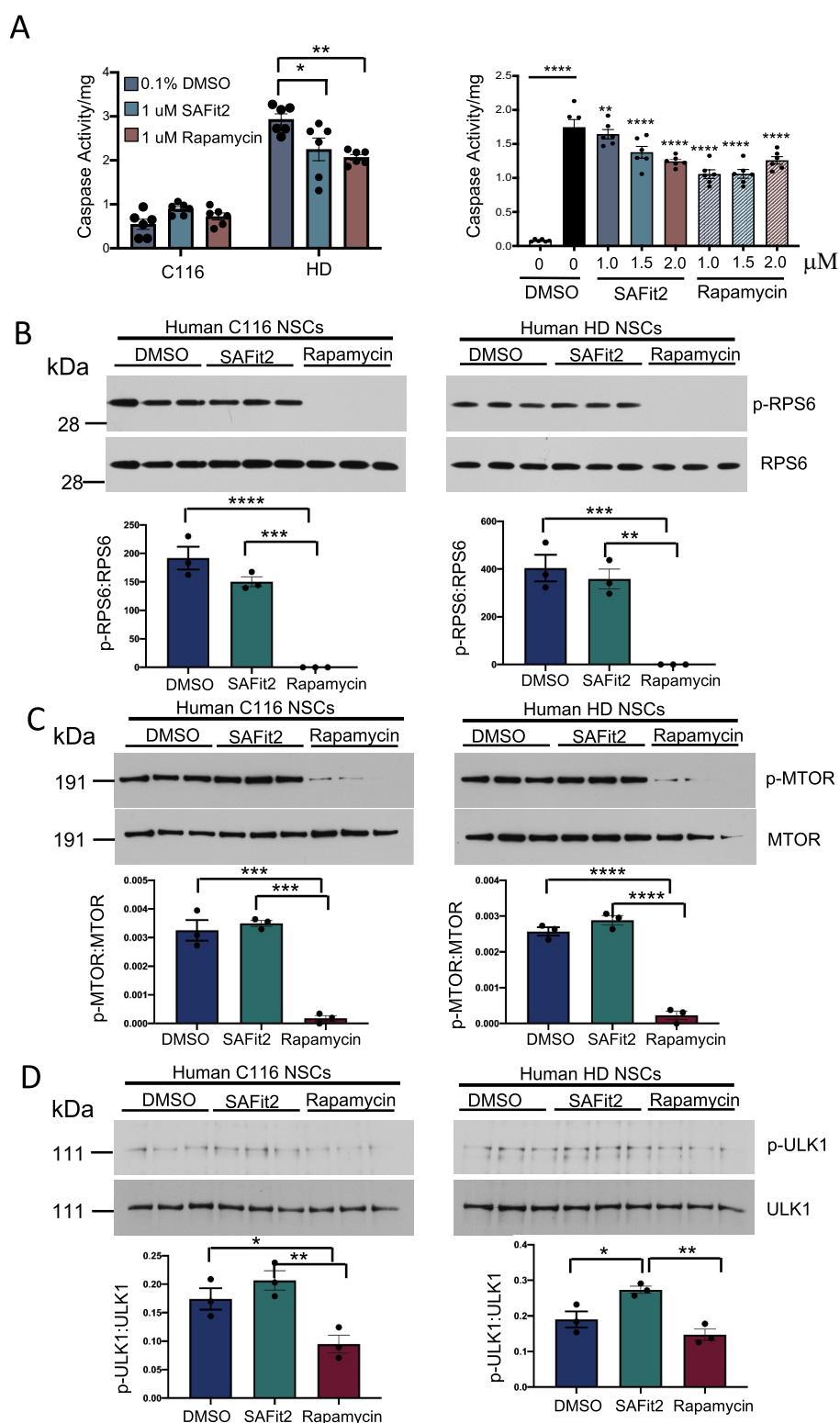
Figure 10. Comparing SAFit2 and rapamycin in HD NSC. (A) Left panel. CASP3-CASP7 activity normalized to protein levels in C116 and HD NSC treated for 24 h in starvation medium with 0.1% DMSO vehicle, 1 µM SAFit2 (two-way ANOVA, *p ≤ 0.05), or 1 µM rapamycin (two-way ANOVA, **p ≤ 0.01). right panel. CASP3-CASP7 activity normalized to protein levels in HD NSC treated for 24 h in starvation media with 0.1% DMSO vehicle, 1, 1.5 and 2 µM SAFit2 (two-way ANOVA, **p ≤ 0.001), or 1, 1.5, and 2.0 µM rapamycin (two-way ANOVA, ***p ≤ 0.001). The two first bars on the left are full media (NPM), media with 0.1% DMSO vehicle, and starvation medium with 0.1% DMSO vehicle. (B,C,D) Quantification of the expression levels of p-RPS6 (B), p-MTOR (C), and p-ULK (D) in C116 and HD NSC after 48 h of treatment with either 0.1% DMSO vehicle, 10 µM SAFit2, or 10 µM rapamycin treatment. analysis of quantified levels indicates significant reduction in phosphorylated RPS6 with 10 µM rapamycin (one-way ANOVA, ****p ≤ 0.0001, and one-way ANOVA, ***p ≤ 0.001) in C116 and HD NSC, respectively, when compared to vehicle control. SAFit2 treatment did not significantly alter levels of phosphorylated RPS6 when compared to control. Analysis of quantified levels indicates significant reduction in phosphorylated MTOR with 10 µM rapamycin (one-way ANOVA, ***p ≤ 0.001, and one-way ANOVA, ****p ≤ 0.0001) in C116 and HD NSC, respectively, when compared to vehicle control.Again, SAFit2 treatment did not significantly alter levels of phosphorylated MTOR when compared to control. analysis of quantified levels indicates significant reduction in phosphorylated ULK1 with 10 µM rapamycin in C116 NSC (one-way ANOVA, *p ≤ 0.05). In HD NSC, treatment with 10 µM SAFit2 significantly increased phosphorylated ULK1 (one-way ANOVA, *p ≤ 0.05) when compared to control.

of HD resulted in the lowering of mHTT levels. The levels of other FKBP family members (e.g., FKBP4, FKBP1A or FKBP1B) were unchanged or modest in mouse and human models of HD.

FKBP5 and HTT co-immunoprecipitated in extracts from multiple brain regions (striatal, cortex and midbrain) of WT and zQ175 mice. Furthermore, studies with confocal microscopy indicated that FKBP5 and mHTT co-localize in the striatum and cortex of WT and zQ175 mice. The interaction of FKBP5 and mHTT may influence the amount of soluble FKBP5 or mHTT in cells. The interaction could be through the proline-rich regions in HTT, and these interactions could influence both the conformation and the aggregation of mHTT [40–42]. The reduction of aggregates in the R6/2 mice treated with a high dose of SAFit2 supports this hypothesis. Further analyses are needed to determine how and if FKBP5 interacts differently with the normal vs. mHTT and if it contributes to protein accumulation and aggregate formation in HD.

FKBP expression is also altered in AD and PD patients and models [67,68]. Pharmacological and genetic inhibition of FKBPs reduces the levels of α-synuclein aggregates and toxicity in PD mouse models [36–38]. Recently, studies showed that FKBP1A enhances calcineurin phosphatase activity toward proteins affected by overexpression of alpha-synuclein; deletion or pharmacological inhibition of FKBP1A, restored phosphorylation of these proteins and reduced cell toxicity [69]. In AD, FKBPs and other PPIases are thought to regulate pathology through their interaction with MAPT protein. MAPT contains multiple phosphorylation sites that determine its function and disease state. MAPT is hyperphosphorylated in AD. It is worth noting that many of the phosphorylation sites in MAPT are located in proline-rich domains. These domains are targeted by PPIases, causing structural changes that render the proteins more stable and thus hinder their clearance [59]. HTT also contains multiple proline domains adjacent to the polyQ tract. The proline domains modulate aggregation and toxicity of mHTT [39,70,71]. Furthermore, a recent study in cellular and nematode models of HD found that increasing levels of FKBP1A changes the structure of the aggregates and reduces their toxicity, suggesting that FKBPs regulate structural changes of mHTT [72]. Our studies did not show dysregulation of FKBP1A across the models tested, but our results support the notion that FKBP family members have an active role in regulating the structure and stability of proteins associated with neurodegenerative diseases.

Reduced levels of mHTT correlates with a reduction in HD pathology [73–76]. Several approaches have been used to specifically suppress production of mHTT and others have focused on the clearance of mHTT [77,78]. Linker molecules that interact with both mHTT and LC3 can increase clearance of mHTT and reduce pathology in cellular and animal models of HD [79]. The degradation of mHTT is impaired at several steps in autophagy, including cargo loading, trafficking of autophagosomes and decreased fusion between autophagosomes and lysosomes [73,80]. Our results suggest that the mHTT can be processed by autophagy upon lowering of FKBP5 expression or activity. The mHTT conformation that impairs these processes in autophagy is likely correlated with proline isomerization (See model Figure 12). Alternatively normal HTT regulates autophagy, and lowering FKBP5 expression or activity restores the function of the mHTT [81]. We show that clearance of HTT is likely due to increased autophagy, as indicated by increased LC3 levels, autophagic flux and change in ULK1 phosphorylation in our HD cellular model. Our results suggest that rapamycin and SAFit2 are both neuroprotective, but the mechanism of autophagy induction are distinct. SAFit2 induction is MTOR independent under normal growth conditions. Further studies are needed to elucidate the impact of the ULK1 pathway by SAFit2 inhibition. Rapamycin as expected inhibited MTOR and activated autophagy.

Previous studies have linked FKBP5 to the autophagy pathways. Gassen et al. showed that increasing FKBP5 levels primed autophagic pathways, and this correlated with the ability of an antidepressant to induce autophagic pathways [82]. They suggest the mechanism for this effect involves a physical interaction of FKBP5 with BECN1 that facilitates autophagy. In this study, changes in autophagic pathways were detected in the presence of antidepressants. Comparison of the autophagic markers in WT and FKBP5 knockout mice were not altered in rested/basal conditions, and therefore, the cellular signaling pathways elicited by antidepressants may not overlap with the effects of FKPB51 on polyQ-expanded HTT in our study.

In summary, we found that FKBP5 levels are altered in HD and that lowering the levels of FKBP5 reduced mHTT in HD models both *in vitro* and *in vivo*, suggesting FKBP5 as a therapeutic target for HD. Notably, FKBP5 knockout murine models exhibit few phenotypic changes or behavioral alterations [23,83] supporting the modulation of FKBP5 as a therapeutic target for neurological diseases. Our results suggest a model in which lowering the levels or activity of FKBP5 leads to increased autophagy, a structural change in the HTT protein likely due to a change in a proline site(s) in the protein and subsequent clearance of the protein (Figure 12). Future studies will systematically evaluate if pharmacological or genetic modulation of this enzyme is beneficial in preclinical studies using HD mouse models.

Materials and methods

Control and HD NSC cultures

NSC were derived and cultured as described [22]. After harvesting from rosettes, NSC were grown on Matrigel (Corning, CB40,234)-coated dishes in Neural Proliferation Medium (Life Technologies,21,103–049). Neurobasal medium was supplemented with 1XB27 (Life Technologies, 17,504–044), 2 mM L-glutamine (Gibco, 35,050–061), 10 ng/mL leukemia inhibitory factor (Peprotech, 300–05), 25 ng/mL bFGF (Peprotech, 100–18B), and 1% penicillin-streptomycin (Corning, 15,140–122). NSC were passaged with Accutase (A11105-01) every 7 d, passaging at a 1:3 ratio. Lysates were harvested by cell scrapping in MPER (Thermo Fisher Scientific, 78,501) with Complete Mini protease inhibitor cocktail (MilliporeSigma, 11,836,170,001), 1% phosphatase Inhibitor Set II (EMD Millipore, 524,625), 1% phosphatase Inhibitor Set III (EMD Millipore, 539,134), 50 μM
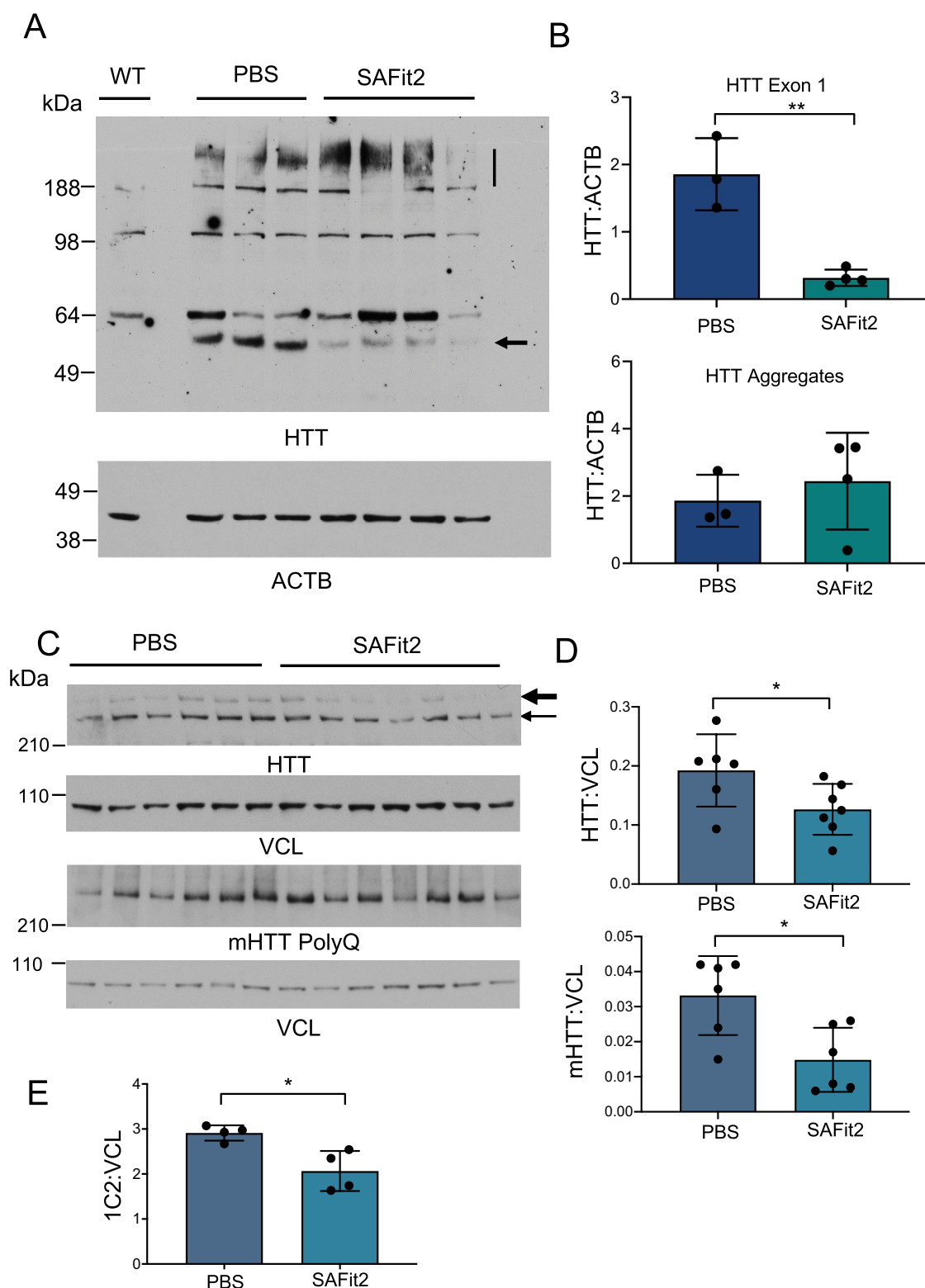
Figure 11. HTT levels in R6/2 and zQ175 mouse models treated with SAFit2. (A) A representative western blot showing HTT exon1 expression and aggregates in R6/2 mice treated with SAFit2, 7.5 mg/kg or vehicle (PBS) for 7 days in the striatum. WT are control is followed by an empty lane. the arrow indicates the polyQ-expanded HTT fragment. the line is the insoluble HTT aggregates that form in the R6/2 mouse. HTT antibody (MilliporeSigma, 5492) was used. (B) Quantification showing a decrease in exon 1 fragments of HTT in R6/2 mice treated with SAFit2 or PBS normalized to ACTB (t-test, **p ≤ 0.01). No significant differences were observed in HTT aggregates. (C) Representative western blot showing expression of HTT, and mHTT normalized to VCL in heterozygote zQ175 mice treated with SAFit2, 15 mg/kg or vehicle (PBS) for 14 days. the thick arrow is the mHTT and the light arrow is WT HTT. (D) Quantification showing normal and mHTT decrease in mice treated with SAFit2 compared to vehicle treated controls (t-test, *p ≤ 0.05). The heavy arrow indicates where mHTT migrates and the lower light arrow is normal HTT. HTT antibody (1:500; MilliporeSigma, MAB5492) was used. (E) Quantification of mHTT using the polyQ antibody 1C2 normalized to VCL showing decreased levels in mice treated with SAFit2 compared to vehicle treated controls (t-test, *p ≤ 0.05).
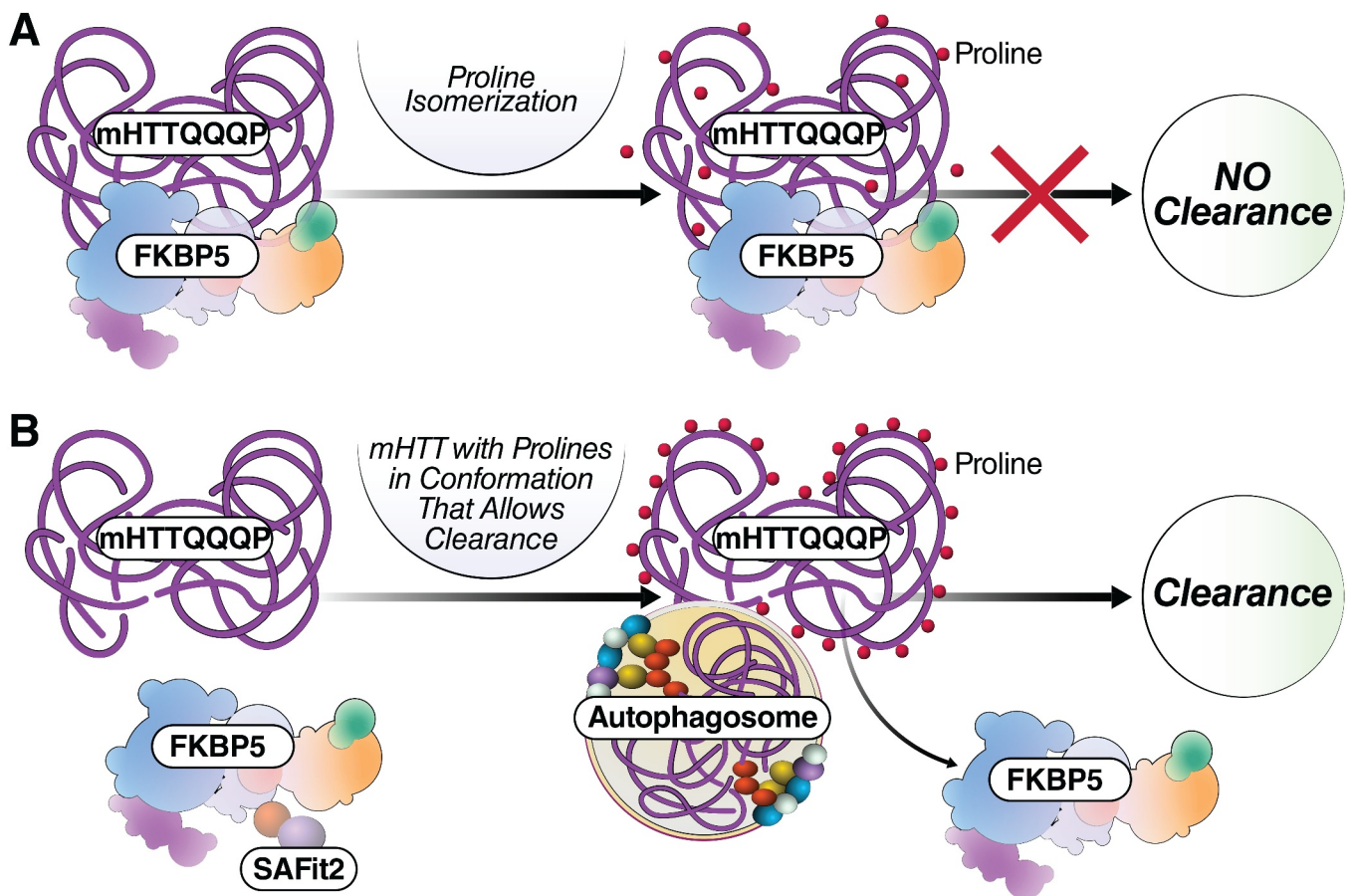
Figure 12. Model of the potential mechanism of clearance of HTT with FKBP5 modulation. (A) The physical interaction and proline isomerization activity of FKBP5 with HTT leads to a conformation of mHTT that is not cleared by autophagy. (B) Decreasing the physical interaction and/or proline isomerization activity of FKBP5 with HTT leads to a conformation state of mHTT that can be cleared by autophagy. This can be mediated by SAFit2 or knockdown of FKBP5.

tricostatin A (MilliporeSigma, T8552), 30 μM sodium butyrate (MilliporeSigma, 303,410), and 30 mM nicotinamide (MilliporeSigma, 72,340). Lysate was sonicated once at 40 mA with 5 s pulses, 5X, with 5 s breaks between each pulse. Sonicated lysate was then centrifuged at 15,294 g for 20 min at 4° C. The supernatant was transfer to a new tube. Protein concentration of the supernatant was determined using the BCA assay (Thermo Fisher Scientific, 23,252).

Transcriptomic analysis of HD NSC

We used our published RNA-seq data set to analyze the changes in mRNA of FKBP family members [84].

siRNA knockdown of FKBP5 in NSC

HD and C116 NSC were cultured as described above. Cells were plated at a density of 100,000 per cm^2 on Matrigel (Corning, CB40234)-treated six-well plates. Cells were transfected at about 90% confluency. Before transfection, the medium was changed to antibiotic-free medium. siRNAs (Dharmacon, FKBP5: J-004224009, non-targeting 001206–13-20) were diluted into a stock solution of 10,000 nM, and 3 μL was used per well in a six-well plate (25 nM per well). The siRNA was complexed with 6 μL of siLentFect Lipid reagent (Biorad, 170–3361). The siRNA and

siLentFect were incubated for 20 min at room temperature (RT) and then slowly added dropwise to the well, and the plate was gently swirled. Fresh antibiotic-free medium was applied 48 h after transfection, and the cells were harvested 96 h after transfection on ice. Cells were rinsed twice with DPBS (Corning, 21–031-CV) and then collected by scrapping in MPER (Thermo Fisher Scientific, 78,501) with Complete Mini protease inhibitor cocktail (MilliporeSigma, 11,836,170,001), 1% Phosphatase Inhibitor Set II (EMD Millipore, 524,625), and 1% Phosphatase Inhibitor III (EMD Millipore, 539,134). Protein concentrations were determined using the BCA assay (Thermo Fisher Scientific, 23,252).

Treatment with SAFit2 in NSC

SAFit2 (Aobious, AOB6548) was dissolved in dimethyl sulfoxide (DMSO, MilliporeSigma, D2650) to a final concentration of 10 mM. Isogenic NSC, HD and C116 (N = 4 per genotype), were treated with DMSO, 1 μM SAFit2, and 10 μM SAFit2. SAFit2 was added to fresh culture medium and then added to the six-well plates as part of the medium change. Cells were harvested 48 h after SAFit2 treatment on ice, rinsed 2X with DPBS and then scrapped with 200 μL of DPBS, and collected by centrifugation at 15,294 x g, and the pellets were frozen. Pellets were resuspended in MPER (Thermo Fisher Scientific, 78,501) and 1X Protease Inhibitor

cocktail (MilliporeSigma, 1,183,670,001). Lysates and protein determinations were carried out as described above.

MSN culture

Activin A (25 ng/mL, Peprotech, AF-120-14E)-treated HD and C116 NSC were used to prepare MSN. Nunc six-well plates were treated with poly-D-lysine hydrobromide (1 mL, 100 μg/mL; MilliporeSigma, P6407) and incubated (37°C and 5% CO_2) overnight (ON). Plates were washed once (1 mL, Corning cell culture grade water, 25–055-CVC) and left to air dry for 1 h inside the culture hood. Next, the plates were treated with Matrigel (1 mL, 50 μg; Corning, CB-40234) ON in an incubator. MSN were prepared according to Kemp et al. [85]. Isogenic HD and C116 MSN were cultured in 6-cm dishes (N = 3 per genotype). Cells were harvested on ice rinsed 1X with neurobasal A medium (Gibco, 10,888–022) and scrapped in MPER lysis buffer described above.

Maintenance and breeding of zQ175 and R6/2 mice

The Buck Institute animal facility is an AAALAC international-accredited institution (Unit #001070). All procedures were approved by the Institutional Animal and Use Committee (A4213-01). Mice were genotyped by PCR analysis with GoTaq Green (Promega, M7121). DNA extraction from isolated tail snips of 3-week-old mice was performed, following the manufacturer's protocol (DNeasy Blood & Tissue kit; Qiagen, 69,504). For zQ175 mice, 8 pmol of PCR control (F: 5′-CATTCATTGCCTTGCTG CTAAG-3′, R: 5′-CTGAAACGACTTGAGCGACTC-3′) and sequence specific primers (IDT) NeoF (F: 5′ GATCGG CCATTGAACAAGATG-3′ R: 5′AGAGCAGCCGATTG TCTGTTG-3′), were used to amplify genomic DNA (50 ng). Cycle conditions were: 96°C 10 min, 35 cycles of 96° C 30 s, 58°C 30 s, 72°C 30 s, followed by a 7-min incubation at 72°C. Samples were run on a 2% agarose gel, positive mice yielded reaction products of the following lengths which distinguishes WT, heterozygote, and homozygote zQ715 mice. R6/2 mice were genotyped, and CAG length was carried out by Laragen.

SAFit2 treatment of R6/2 and zQ175 mice

SAFit2 (Aobious, AOB6548) was reconstituted in 100% EtOH to a concentration of 0.1 mg/μl and stored at −20°C. On the day of injection, the SAFit2 stock was diluted to the desired concentration in a final solution with the following totals of 4% EtOH, 5% Tween 80 (MilliporeSigma, P4780), 5% PEG400 (MilliporeSigma, 8.07485) in 0.9% saline. It is worth noting that the SAFit2 must be brought up to the final 4% EtOH before the remaining components can be added. Mice were injected with 100 μL volume of either the SAFit2 solution or the buffer solution (4% EtOH, 5% Tween 80, 5% PEG400 in 0.9% saline). Animals were daily intraperitoneal injected, and 4 h before harvest. Injection sites were altered between the left or right side daily.

Mouse brain dissection and homogenization

To collect mouse brains, mice were anesthetized with isoflurane (Butler Schein, 1,040,603) and cervically dislocated. An adult brain matrix (Bioanalytical Systems, RBM-2000 c) was used to section the brain into 1-mm coronal slices. Cortical and striatal regions were dissected from these slices. All dissections and brain collections were performed on ice and flash frozen on dry ice. Samples were store at 80°C ON or until tissue homogenization. Lysis (200 μL striatum, 400 μL cortex) was performed with T-PER™ tissue protein extraction reagent (10 mL; Thermo Fisher Scientific,78,510) containing protease inhibitors (Complete Mini; MilliporeSigma, 11,836,170,001, 1 tablet/10 mL), DNAase (1 μL; Invitrogen, EN0521), $MgCl_2$ (1.2 mM; Honeywell Fluka, 60–047-233), epoxomycin (1 μM; MilliporeSigma, E3652), Phosphatase Inhibitor Cocktail II (100 μL, PPI II; Calbiochem, 524,625), tricostatin A (50 μM; MilliporeSigma, T8552), nicotinamide (30 mM; Sigma-Aldrich, 72,340) and sodium butyrate (30 μM; MilliporeSigma, 303,410). A dounce homogenizer (2 mL; Kimble Chase, KT885300-0002) was used for tissue homogenization (2 X 60 pumps with a 30-s interval) on ice. After homogenization samples were stored at −80°C. Lysates were sonicated 3X at 40 mA with 5-s pulses, 5X, with 5-s breaks between each pulse. Sonicated lysates were subjected to centrifugation at 15,294 x g or 20 min at 4°C. Supernatants were saved in a new tube, and the debris pellets were discarded. Protein concentrations of the supernatant were determined using the BCA assay (Thermo Fisher Scientific, 23,252).

Western blot analysis for FKBP5 siRNA knockdown in NSC

Lysates (8–15 μg) were prepared in 4X sample buffer (Invitrogen, NP0007) with 0.05 M DTT, and boiled for 10 min at 95°C. Lysates were run on a 4–12% Bis-tris gel at 200 V for 50 min in MES running buffer (Invitrogen, NP0002) with antioxidant (Invitrogen, NP0005). Transfer was performed ON, 20 V for 840 min at 4°C, onto a 0.4-μm nitrocellulose membrane. Blocking was done with 5% milk in 1X TBST (Teknova, T9511). After blocking membranes were probed with the following primaries: FKBP5/FKBP5 (1:100; Cell Signaling Technology, 12,210), HTT (Millipore, MAB2166), polyQ 1C2 (1:500; Millipore, MAB1574), VCL/ vinculin (1:500; MilliporeSigma, V9131) or ACTB/β-actin (1:-1000–2000; MilliporeSigma, A5441). Membranes were incubated with secondary anti-murine horseradish peroxidase (HRP)-coupled antibodies (1:2500; GE Healthcare, NXA931) or anti-rabbit HRP-coupled antibodies (1:2500; GE Healthcare, NA934 at RT for 2 h in 5% milk TBST solution. Protein bands were detected by chemiluminescence (Pierce ECL; Thermo Fisher Scientific, 32,106). ImageQuant TL (v2005, Amersham Biosciences) was used for densitometry analysis.

Western blot analysis for FKPB51 in NSC and MSN treated with SAFit2

Lysates (8–15 μg) were prepared in 4X sample buffer (Invitrogen, NP0007) with 0.05 M DTT, and boiled for 10 min

at 95°C. Lysates were run on a 4–12% Bis-tris gel at 200 V for 50 min in MES running buffer (Invitrogen, NP0002) with anti-oxidant (Invitrogen, NP0005). Transfer was performed ON, 20 V for 840 min at 4°C, onto a 0.4-μm nitrocellulose membrane. Blocking was done with 5% milk in TBST. After blocking membranes were probed with the following primaries: FKBP5/FKBP5 (1:100; Cell Signaling Technology, 12,210), VCL/vinculin (1:500; MilliporeSigma, V9131) or ACTB/β-actin (1:1000–2000; MilliporeSigma, A5441), or TUBA4A/TUBA1A/α-tubulin (1:1000; MilliporeSigma, T6199). Membranes were incubated with secondary anti-murine HRP-coupled antibodies (1:2500; GE Healthcare, NXA931) or anti-rabbit HRP-coupled antibodies (1:2500; GE Healthcare, NA934) at RT for 2 h in 5% milk TBST solution. Protein bands were detected by chemiluminescence (Pierce ECL; Thermo Fisher Scientific, 32,106). ImageQuant TL (v2005, Amersham Biosciences) was used for densitometry analysis.

Western blot analysis of HTT and mHTT in HD NSC and MSN

Lysates (20 μg) were prepared in 4X sample buffer (Invitrogen, NP0007) with 0.05 M DTT, and boiled for 10 min at 95°C. mHTT and HTT bands were separated on a 3–8% Tris-acetate gel, run for 90 min in Tris-acetate running buffer (Invitrogen, LA0041) and antioxidant (Invitrogen, NP0005) at 200 V on ice. Transfer was performed at 4°C at a constant 20 V for 840 min in transfer buffer (Thermo Fischer Scientific, NP00061) onto a nitrocellulose membrane. Blocking was done ON in 5% milk in TBST, primary antibody HTT (1:250; Millipore MAB2166), HTT (1:500; Millipore, 1574), VCL/vinculin (1:500; MilliporeSigma, V9131) was probed at 4°C ON in 5% milk TBST, secondary HRP-coupled anti-mouse (GE Healthcare, NXA931; 1:2500) was probed ON at 4°C in 5% milk TBST. Protein bands were detected by chemiluminescence (Pierce ECL; Thermo Fisher Scientific, 32,106). ImageQuant TL (v2005, Amersham Biosciences) was used for densitometry analysis.

LC3 Western blots

Protein concentrations were determined by BCA protein assay (Thermo Fisher Scientific, 23,225). Lysates (5 μg) were prepared in 4X LDS buffer (Invitrogen, NP0007) and 0.05 M DTT. Samples were boiled for 10 min at 95°C and separated by 1D-SDS-PAGE electrophoresis on a 12% Bis-Tris gel at 200 V for 60 min in MOPS running buffer and antioxidant (Invitrogen, NP0005). Transfer was performed on ice in a cold room at 350 mA constant for 1 h in transfer buffer (Invitrogen, NP00061) with 10% methanol onto a 0.2-μm PVDF membrane (Millipore, LC20002). After blocking in 5% milk in TBST, primary antibody (20 μg/ml; Novous, 100–2220) was incubated ON in 5% milk in TBST at 4°C. Membranes were incubated with secondary anti-rabbit (1:2500; GE Healthcare, NA934) or anti-murine (NXA931) HRP-coupled antibodies (1:2500; GE Healthcare) at RT for 2 h in 5% milk TBST solution. Protein bands were detected by chemiluminescence (Pierce ECL; Thermo Fisher Scientific, 32,106). ImageQuant TL (v2005, Amersham Biosciences) was used for densitometry analysis.

Western blot analysis comparing SAFit2 and rapamycin treatment in NSC

Lysates (15 μg) were prepared in 4X sample buffer (Invitrogen, NP0007) with 0.05 M DTT, and boiled for 10 min at 95°C. Bands were separated on a 3–8% Tris-acetate gel, run for 90 min in Tris-acetate running buffer (Invitrogen, LA0041) and antioxidant (Invitrogen, NP0005) at 200 V on ice. Transfer was performed at 4°C at a constant 20 V for 840 min in transfer buffer (Invitrogen, NP00061) onto a nitrocellulose membrane. Blocking for all phosphorylated antibodies was done ON in 5% BSA (MilliporeSigma, 03117332001) in TBST. Blocking for all non-phosphorylated equivalents of antibodies was done ON in 5% milk in TBST. Primary antibody phosphorylated MTOR (1:100; Cell Signaling Technology, 2971), was normalized to total MTOR (1:100; Cell Signaling Technology, 2972). Both antibodies were applied at 4°C ON in 5% milk TBST or 5% BSA TBST, secondary HRP-coupled anti-rabbit (1:3000; GE Healthcare, NA934). Further comparison was done by probing primary antibodies phosphorylated ULK1 (1:100: Cell Signaling Technology, 6888) probed at 4°C ON in 5% BSA TBST, normalized to total ULK1 (1:100; MilliporeSigma, 7481), probed at 4°C ON in 5% milk TBST. Both antibodies utilized secondary HRP-coupled anti-rabbit (1:3000; GE Healthcare, NA934) and were probed ON at 4°C in 5% BSA or milk TBST, respectively. A 4–12% Bis-Tris gel, run for 50 min in Tris-acetate running buffer (Invitrogen, LA0041) and antioxidant (Invitrogen, NP0005) at 200 V on ice was used for RPS6/S6. Primary antibodies utilized for probing were phosphorylated RPS6 (1:100; Cell Signaling Technology, 5364) probed at 4°C ON in 5% BSA TBST, normalized to total S6 (1:100; Cell Signaling Technology, 2217), probed at 4°C ON in 5% milk TBST. Both antibodies utilized secondary HRP-coupled anti-rabbit (1:3000; GE Healthcare, NA934) and were probed ON at 4°C in 5% BSA or milk TBST, respectively. Protein bands were detected by chemiluminescence (Pierce ECL; Thermo Fisher Scientific, 32,106). ImageQuant TL (v2005, Amersham Biosciences) was used for densitometry analysis.

Caspase activity assay comparing SAFit2 to rapamycin treatment in NSC

A 96-well assay plate with black sides and clear flat bottom (Corning, 3340) was coated with Matrigel solution in DMEM F-12 Knockout medium (50 μL/well), and allowed to sit for 24 h at 37°C. NSC were seeded at 20,000 cells/well, and allowed to culture in NPM until achieving 70% confluency. Cells were then treated with 0.1% DMSO (NBM with 1% penicillin-streptomycin), SAFit2, or rapamycin in starvation media, for 24 h. After 24 h, Activated Caspase APO 3/7 HTS kit (Cell Technology, APO200-3), including Cell lysis buffer (3005), and Caspase 3/7 Reagent (z-DEVD) 2 Rodamine 110 (Cell Technology, 4004). Change in fluorescence was recorded on a PerkinElmer VictorX3 Multimode Plate Reader. One hundred reads at 488 nm emission were collected, and a best fit line was calculated through the reads. The best fit line was then normalized to total protein value calculated by

BCA assay on a by well basis to calculate the Caspase Activity/total Protein.

Western blotting for FKBPs in HD transgenic mice brain lysates

Cortical and striatal lysates (20–40 μg) were prepared in 4X LDS buffer (Invitrogen, NP0007) and 0.05 M DTT. Samples were boiled for 10 min at 95°C and separated by 1D-SDS-PAGE electrophoresis on a 12% Bis-Tris gel at 200 V for 50 min in MOPS running buffer and antioxidant (Invitrogen, NP0005). Transfer was performed on ice in a cold room at 350 mA constant for 1 h in transfer buffer (Invitrogen, NP00061) with 10% methanol onto a 0.2-μm PVDF membrane (Thermo Fisher, 88,520). After blocking in 5% milk in TBST, primary antibody FKBP1A/FKBP12 (1:1000–4000; Abcam, ab2918), FKBP1B/FKBP12.6 (1:100–200, Abcam, ab82316); FKBP5/FKBP51 (1:100–500; Cell Signaling Technology, D5G2), FKBP4/FKBP52 (1:100; Cell Signaling Technology, 11,826), TUBA4A/TUBA1A/α-tubulin (1:500–4000; MilliporeSigma, T6199) were incubated ON in either 5% milk TBST or 5% BSA TBST at 4°C. Membranes were incubated with secondary anti-rabbit (1:2500; GE Healthcare NA934) or anti-murine HRP-coupled antibodies (1:2500; GE Healthcare, NXA931) at RT for 2 h in 5% milk TBST solution. Protein bands were detected by chemiluminescence (Pierce ECL; Thermo Fisher Scientific, 32,106). ImageQuant TL (v2005, Amersham Biosciences) was used for densitometry analysis.

Western blot analysis in R6/2 and zQ175 treated with SAFit2

Lysates (15–30 μg) were prepared in 4X sample buffer (Invitrogen, NP0007) with 0.05 M DTT, and boiled for 10 min at 95°C. The R6/2 lysates were run on a 4–12% Bis-tris gel at 200 V for 50 min in MES running buffer (Invitrogen, NP0002) with antioxidant (Invitrogen, NP0005). The zQ175 lysates were separated on 3–8% tris-acetate gel at 200 V for 90 min in tris-acetate running buffer. Transfer was performed ON, 20 V for 840 min at 4°C, onto a 0.4-μm nitrocellulose membrane. Blocking was done with 5% milk in TBST. After blocking membranes were probed with the following primaries: HTT (1:500; MilliporeSigma, 5492), FKBP5/FKBP51 (1:100; Cell Signaling Technology, 12,210), VCL/vinculin (1:500; MilliporeSigma, V9131) or ACTB/β-actin (1:1000–2000; MilliporeSigma, A5441), or TUBA4A/TUBA1A/α-tubulin (1:1000; MilliporeSigma,T6199). Membranes were incubated with secondary anti-murine HRP-coupled antibodies (1:2500; GE Healthcare, NXA931) or anti-rabbit (1:2500; GE Healthcare, NA934) at RT for 2 h or ON at 4°C in 5% milk TBST solution. Protein bands were detected by chemiluminescence (Pierce ECL; Thermo Fisher Scientific, 32,106). ImageQuant TL (v2005, Amersham Biosciences) was used for densitometry analysis.

IHC staining

Paraffin-embedded coronal mouse brain sections from zQ175 and WT mice (7 μm) were deparaffinized and rehydrated with xylene and ethanol rinses, with a final rinse in deionized water. The slides were then washed in TBS for 10 min. Antigen retrieval was performed using citrate buffer at pH 6.0 for 5 min at 40% power in 1100 W microwave (Sanyo). The slides were allowed to cool in the same buffer at RT for 20 min. Slides were then washed in TBS. Sections were blocked for 60 min in blocking buffer containing 5% normal goat serum in TBS and 2 μg/mL goat anti-mouse IgG (1 mg/ml; Aves Labs, Inc., IMU-1010). Primary antibodies FKBP5/FKBP51 (1:25; Santa Cruz Biotechnology, sc-271,547) and HTT (1:50; MilliporeSigma, H7540) were diluted in 1% BSA in TBS and left at 4°C ON in a humidified chamber. Slides were washed three times in TBS. Secondary antibodies of goat-anti mouse Alexa Fluor 555 (1:500; Thermo Fisher Scientific, A21424) and goat-anti rabbit Alexa Fluor 488 (1:500; Thermo Fisher Scientific, A11006) were diluted in 1% BSA in TBS and incubated at RT for 2 h. Slides were washed for 10 min, three times and then dried. Slides were mounted using Prolong Gold with DAPI (Thermo Fisher Scientific, P36931). All images were collected using a Zeiss LSM 780 confocal on an Axio Observer Z1 inverted microscope with Plan-Apochromat 63x/1.40 NA Oil DIC objective and zoom at 2.0. DAPI was excited with a 405-nm Diode laser line at 36.8% (Filter 410–498 nm). Alexa Flour 488 secondary was excited with a 488-nm Argon laser line at 2.5% (Filter 490–544 nm). Alexa Fluor 555 secondary was excited with a 555 nm DPSS laser line at 10.0% (Filter 566–697 nm). Master gain for all channels set to 650. Dimensions: x: 1584, y: 1584, z: 25, channels: 3, 12-bitImage size x: 71.03 μm, y: 71.03 μm, z: 7.74 μm. Z-series optical sections were collected with a step-size of 0.28 μ in 26 steps over 7 μ in the z dimension. Co-localization analysis was done using IMARIS 64 software (IMARIS x64 7.4.2 February 2021 2012 Build 26,649 for x64, Bitplane Scientific Software).

Co-immunoprecipitation with HTT or FKBP5 antibody

Total midbrain lysate was used from homozygote zQ175 and wild-type mice for Co-IP. Co-IP for striatal and cortical lysates used an allelic series of heterozygote mice consisting of WT, 50Q, 90Q, and 175Q expansions. Total lysate (300 μg, midbrain, striatal or cortical) was diluted into a final volume of 700 μL (T-PER, Thermo Fisher Scientific, 78,510; Protease Inhibitor Complete tablet, MilliporeSigma, 11,697,498,001). The lysate was pre-cleared with protein G beads (GE Healthcare, 17,061,801) for 1 h at 4°C. Pre-cleared brain lysates were incubated ON at 4°C with HTT antibody (1:140; Millipore, MAB2166) or FKBP5 antibody (1:50; Cell Signaling Technology, 12,210) or no antibody as a control. Lysate was incubated with protein G beads (GE Healthcare, 17,061,801) for 5 h at 4°C. Beads were washed with TPER (5X) and eluted with 2X LDS buffer (50 μL; Invitrogen, NP0007) and 0.1 M DTT, boiled for 10 min and then spun at 15,294 x g for 10 min,

and the supernatant was saved. Twenty-five µL of the total 50 µL elute volume was boiled for 10 min at 95°C and then separated by 1D-SDS PAGE electrophoresis on a 4–12% Bis-Tris gel at 200 V for 50 min in MES running buffer (Invitrogen, NP0002) with antioxidant (Invitrogen, NP0005). Transfer was performed ON, 20 V for 840 min at 4°C, onto a 0.4-µm nitrocellulose membrane. Blocking was done with 5% milk in TBST. After blocking primary antibody of HTT (1:100–300; Millipore, MAB2166) and FKBP5/FKBP51 (1:100–250; Cell Signaling Technology,12,210) and FKBP5/FKBP51 (1:100–300; Santa Cruz Biotechnology, 271,547) was incubated ON at 4°C in 5% milk in TBST. Membranes were incubated with secondary anti-rabbit (1:2500; GE Healthcare, NA934V) or anti-murine (1:2500; GE Healthcare, NXA931) HRP-coupled antibodies at RT for 2 h or ON at 4°C in 5% milk TBST solution. Protein bands were detected by chemiluminescence (Pierce ECL; Thermo Fisher Scientific, 32,106). ImageQuant TL (v2005, Amersham Biosciences) was used for densitometry analysis.

Immunocytochemistry of NSC

NSC were cultured in eight-well Matrigel (Corning, CB40234)-coated-chamber slides eight-well chamber slides (BD Falcon, 354,108) and fixed with 4% PFA (MilliporeSigma, 158,127) for 15 min at RT and washed three times with PBS (corning, 21–031-CV). Cells were permeabilized with 0.1% Triton X-100 (Fisher Scientific, BP151-100) in PBS PBS (corning, 21–031-CV). Blocking was done with 1% BSA (MilliporeSigma, 03117332001) and 5% donkey serum (MilliporeSigma, D9663) in PBS. Primary antibodies (1:200, FKBP5, Santa Cruz Biotechnology, sc-271,547; 1:200, HTT, MilliporeSigma, H7540) were incubated for 24 h at 4°C in a humid chamber. Secondary antibodies (Alexa 488 and Alexa 546) were used at 1:250 at RT for 90 min in the dark. Slides were mounted with 1.5-mm coverslips and ProLong Gold with DAPI antifade mount. Imaging was done on a Nikon Eclipse Ti-U microscope using Plan Apo λ 20X/ 0.75 objective.

Immunocytochemistry of human MSN

C116 and HD MSN were fixed using 4% paraformaldehyde in 0.1 M PBS, pH 7.4 (Corning, 21–040-CV) for 30 min. After three washes in PBS, cells were permeabilized and blocked for 1 h at RT using 0.1% Triton X-100 (Thermo Fisher Scientific, 28,313) and 4% donkey serum in PBS. Primary antibodies were added in the presence of blocking buffer ON at 4°C. Secondary antibodies (1:500) were added after three PBS washes in blocking buffer at RT for 1 h. The following primary antibodies were used for the immunofluorescence studies: rabbit anti-PPP1R1B /DARPP-32 (1:100; Santa Cruz Biotechnology, sc-11,365), rabbit anti-MAP2 (1:100; Millipore, AB5622) and rabbit anti-NES/nestin (1:100; Abcam, ab92391). The secondary antibodies were donkey anti-rabbit IgG conjugated with Alexa Fluor 488 (Invitrogen, A12379) or Alexa Fluor 647 (Invitrogen, A22287). Images were acquired using a Biotek

Cytation 5 microscope and were prepared using Fiji software (ImageJ).

Statistical analysis

Student's paired *t*-test and ANOVA with Tukey's multiple comparison test was used to study differences in expression. All statistical analysis and graph plotting were performed using PRISM 7 by GraphPad Software (La Jolla, CA, USA). $p < 0.05$ was considered as statistically significant.

Disclosure statement

The authors have no conflicts of interest to declare.

ORCID

Ningzhe Zhang http://orcid.org/0000-0003-4276-2962
Felix Hausch http://orcid.org/0000-0002-3710-8838

References

[1] Group THsDCR. A novel gene containing a trinucleotide repeat that is expanded and unstable on Huntington's disease chromosomesThe Huntington's Disease Collaborative Research Group. Cell. 1993;72(6):971–983.

[2] Hedreen JC, Peyser CE, Folstein SE, et al. Neuronal loss in layers V and VI of cerebral cortex in Huntington's disease. Neurosci Lett. 1991;133(2):257–261.

[3] Kiyama H, Seto-Ohshima A, Emson PC. Calbindin D28K as a marker for the degeneration of the striatonigral pathway in Huntington's disease. Brain Res. 1990;525(2):209–214.

[4] Cardoso F. Differential diagnosis of Huntington's disease: what the clinician should know. Neurodegener Dis Manag. 2014;4(1):67–72.

[5] Marxreiter F, Stemick J, Kohl Z. Huntingtin lowering strategies. Int J Mol Sci. 2020;21(6):21.

[6] Tabrizi SJ, Leavitt BR, Landwehrmeyer GB, et al. Targeting huntingtin expression in patients with huntington's disease. N Engl J Med. 2019;380(24):2307–2316.

[7] Siekierka JJ, Hung SH, Poe M, et al. A cytosolic binding protein for the immunosuppressant FK506 has peptidyl-prolyl isomerase activity but is distinct from cyclophilin. Nature. 1989;341 (6244):755–757.

[8] Cioffi DL, Hubler TR, Scammell JG. Organization and function of the FKBP52 and FKBP51 genes. Curr Opin Pharmacol. 2011;11(4):308–313.

[9] Van Duyne GD, Standaert RF, Karplus PA, et al. Atomic structure of FKBP-FK506, an immunophilin-immunosuppressant complex. Science. 1991;252:839–842.

[10] Van Duyne GD, Standaert RF, Karplus PA, et al. Atomic structures of the human immunophilin FKBP-12 complexes with FK506 and rapamycin. J Mol Biol. 1993;229(1):105–124.

[11] Hartmann J, Wagner KV, Liebl C, et al. The involvement of FK506-binding protein 51 (FKBP5) in the behavioral and neuroendocrine effects of chronic social defeat stress. Neuropharmacology. 2012;62(1):332–339.

[12] Schreiber KH, Ortiz D, Academia EC, et al. Rapamycin-mediatedmTORC2 mTORC2 inhibition is determined by the relative expression of FK506-binding FK506-binding proteins. Aging Cell. 2015;14(2):265–273.

[13] Hausch F, Kozany C, Theodoropoulou M, et al. FKBPs and the Akt/mTOR pathway. Cell Cycle. 2013;12(15):2366–2370.

[14] Huang S, Pj H. Targeting mTOR signaling for cancer therapy. Curr Opin Pharmacol. 2003;3(4):371–377.

[15] Yao YL, Liang YC, Huang HH, et al. FKBPs in chromatin modification and cancer. Curr Opin Pharmacol. 2011;11(4):301–307.

[16] Gaali S, Kirschner A, Cuboni S, et al. Selective inhibitors of the FK506-binding protein 51 by induced fit. Nat Chem Biol. 2015;11(1):33–37.

[17] Harrar Y, Bellini C, Jd F. FKBPs: at the crossroads of folding and transduction. Trends Plant Sci. 2001;6(9):426–431.

[18] Riggs DL, Cox MB, Tardif HL, et al. Noncatalytic role of the FKBP52 peptidyl-prolyl isomerase domain in the regulation of steroid hormone signaling. Mol Cell Biol. 2007;27(24):8658–8669.

[19] Wochnik GM, Ruegg J, Abel GA, et al. FK506-binding proteins 51 and 52 differentially regulate dynein interaction and nuclear translocation of the glucocorticoid receptor in mammalian cells. J Biol Chem. 2005;280(6):4609–4616.

[20] Wu B, Li P, Liu Y, et al. 3D structure of human FK506-binding protein 52: implications for the assembly of the glucocorticoid receptor/Hsp90/immunophilin heterocomplex. Proc Natl Acad Sci U S A. 2004;101(22):8348–8353.

[21] Blair LJ, Criado-Marrero M, Zheng D, et al. The Disease-Associated Chaperone FKBP51 Impairs Cognitive Function by Accelerating AMPA Receptor Recycling. eNeuro. 2019;6(1). doi:10.1523/ENEURO.0242-18.2019.

[22] Zgajnar NR, De Leo SA, Lotufo CM, et al. Biological Actions of the Hsp90-binding Immunophilins FKBP51 and FKBP52. Biomolecules. 2019;9(2):52. doi:10.3390/biom9020052.

[23] O'Leary JC 3rd, Dharia S, Blair LJ, et al. A new anti-depressive strategy for the elderly: ablation of FKBP5/FKBP51. PLoS One. 2011;6(9):e24840.

[24] Touma C, Gassen NC, Herrmann L, et al. FK506 binding protein 5 shapes stress responsiveness: modulation of neuroendocrine reactivity and coping behavior. Biol Psychiatry. 2011;70(10):928–936.

[25] Albu S, Romanowski CP, Letizia Curzi M, et al. Deficiency of FK506-binding protein (FKBP) 51 alters sleep architecture and recovery sleep responses to stress in mice. J Sleep Res. 2014;23(2):176–185.

[26] Storer CL, Dickey CA, Galigniana MD, et al. FKBP51 and FKBP52 in signaling and disease. Trends Endocrinol Metab. 2011;22(12):481–490.

[27] Uk J, Koren J 3rd, Si B, et al. The Hsp90 cochaperone, FKBP51, increases Tau stability and polymerizes microtubules. J Neurosci. 2010;30(2):591–599.

[28] Criado-Marrero M, Rein T, Binder EB, et al. Hsp90 and FKBP51: complex regulators of psychiatric diseases. Philos Trans R Soc Lond B Biol Sci. 2018;373(1738):373.

[29] Taler-Vercic A, Hasanbasic S, Berbic S, et al. Proline residues as switches in conformational changes leading to amyloid fibril formation. Int J Mol Sci. 2017;18(3):18.

[30] Schmidt U, Buell DR, Ionescu IA, et al. A role for synapsin in FKBP51 modulation of stress responsiveness: convergent evidence from animal and human studies. Psychoneuroendocrinology. 2015;52:43–58.

[31] Daskalakis NP, Binder EB. Schizophrenia in the spectrum of gene-stress interactions: the FKBP5 example. Schizophr Bull. 2015;4130(2):323–9591-9.

[32] Blair LJ, Nordhues BA, Hill SE, et al. Accelerated neurodegeneration through chaperone-mediated oligomerization of tau. J Clin Invest. 2013;123(10):4158–4169.

[33] Boonying W, Joselin A, Huang E, et al. Pink1 regulates FKBP5 FKBP5 interaction withAKT/PHLPP AKT/PHLPP and protects neurons from neurotoxin stress induced byMPP(.)MPP+. J Neurochem. 2019;150(3):312–329.

[34] Li H, Su P, Lai TK, et al. The glucocorticoid receptor-FKBP51 complex contributes to fear conditioning and posttraumatic stress disorder. J Clin Invest. 2020;130(2):877–889.

[35] Matosin N, Halldorsdottir T, Binder EB. Understanding the molecular mechanisms underpinning gene by environment interactions in psychiatric disorders: the FKBP5 model. Biol Psychiatry. 2018;83(10):821–830.

[36] Gerard M, Deleersnijder A, Daniels V, et al. Inhibition of FK506 binding proteins reduces alpha-synuclein aggregation and Parkinson's disease-like pathology. J Neurosci. 2010;30(7):2454–2463.

[37] Gold BG, Nutt JG. Neuroimmunophilin ligands in the treatment of Parkinson's disease. Curr Opin Pharmacol. 2002;2(1):82–86.

[38] Gerard M, Debyser Z, Desender L, et al. The aggregation of alpha-synuclein is stimulated by FK506 binding proteins as shown by fluorescence correlation spectroscopy. Faseb J. 2006;20(3):524–526.

[39] Dehay B, Bertolotti A. Critical role of the proline-rich region in Huntingtin for aggregation and cytotoxicity in yeast. J Biol Chem. 2006;281130(47):15877–15889.

[40] Darnell G, Orgel JP, Pahl R, et al. Flanking polyproline sequences inhibit beta-sheet structure in polyglutamine segments by inducing PPII-like helix structure. J Mol Biol. 2007;374(3):688–704.

[41] Bhattacharyya A, Thakur AK, Chellgren VM, et al. Oligoproline effects on polyglutamine conformation and aggregation. J Mol Biol. 2006;355(3):524–535.

[42] Wetzel R. Physical chemistry of polyglutamine: intriguing tales of a monotonous sequence. J Mol Biol. 2012;421(4–5):466–490.

[43] Wagner AS, Politi AZ, Ast A, et al. Self-assembly of mutant huntingtin exon-1 fragments into large complex fibrillar structures involves nucleated branching. J Mol Biol. 2018;430(12):1725–1744.

[44] Ring KL, An MC, Zhang N, O'Brien RN, Ramos EM, Gao F, et al. Genomic analysis reveals disruption of striatal neuronal development and therapeutic targets in human huntington's disease neural stem cells. Stem Cell Reports. 2015;5(6):1023–1038.

[45] Balsevich G, Hausl AS, Meyer CW, et al. Stress-responsive FKBP51 regulates AKT2-AS160 signaling and metabolic function. Nat Commun. 2017;8(1):1725.

[46] Heikkinen T, Lehtimaki K, Vartiainen N, et al. Characterization of neurophysiological and behavioral changes, MRI brain volumetry and 1H MRS in zQ175 knock-in mouse model of Huntington's disease. PLoS One. 2012;7(12):e50717.

[47] Menalled LB, Kudwa AE, Miller S, et al. Comprehensive behavioral and molecular characterization of a new knock-in mouse model of Huntington's disease: zQ175. PLoS One. 2012;7(12):e49838.

[48] Langfelder P, Cantle JP, Chatzopoulou D, et al. Integrated genomics and proteomics define huntingtin CAG length-dependent networks in mice. Nat Neurosci. 2016;19(4):623–633.

[49] Mangiarini L, Sathasivam K, Seller M, et al. Exon 1 of the HD gene with an expanded CAG repeat is sufficient to cause a progressive neurological phenotype in transgenic mice. Cell. 1996;87(3):493–506.

[50] Cummings DM, Alaghband Y, Hickey MA, et al. A critical window of CAG repeat-length correlates with phenotype severity in the R6/2 mouse model of Huntington's disease. J Neurophysiol. 2012;107(2):677–691.

[51] Menalled L, El-Khodor BF, Patry M, et al. Systematic behavioral evaluation of Huntington's disease transgenic and knock-in mouse models. Neurobiol Dis. 2009;35107(3):319–36677-691.

[52] Menalled LB, Sison JD, Dragatsis I, et al. Time course of early motor and neuropathological anomalies in a knock-in mouse model of Huntington's disease with 140 CAG repeats. J Comp Neurol. 2003;465(1):11–26.

[53] Neto JL, Lee JM, Afridi A, et al. Genetic contributors to inter-generational CAG repeat instability in huntington's disease knock-in mice. Genetics. 2017;205(2):503–516.

[54] Franich NR, Basso M, Andre EA, et al. Striatal mutant huntingtin protein levels decline with age in homozygous huntington's disease knock-in mouse models. J Huntington's Dis. 2018;7(2):137–150.

[55] Reindl W, Baldo B, Schulz J, et al. Meso scale discovery-based assays for the detection of aggregated huntingtin. PLoS One. 2019;14(3): e0213521.

[56] An MC, O'Brien RN, Zhang N, et al. Polyglutamine Disease Modeling: epitope Based Screen for Homologous Recombination using CRISPR/Cas9 System. PLoS currents. 2014;6. doi:10.1371/currents.hd.0242d2e7ad72225efa72f6964589369a.

[57] An MC, Zhang N, Scott G, et al. Genetic correction of Huntington's disease phenotypes in induced pluripotent stem cells. Cell Stem Cell. 2012;11(2):253–263.

[58] Al-Ramahi I, Lu B, Di Paola S, et al. High-throughput functional analysis distinguishes pathogenic, nonpathogenic, and compensatory transcriptional changes in neurodegeneration. Cell Syst. 2018;7(1):28–40 e4.

[59] Blair LJ, Baker JD, Sabbagh JJ, et al. The emerging role of peptidyl-prolyl isomerase chaperones in tau oligomerization, amyloid processing, and Alzheimer's disease. J Neurochem. 2015;133(1):1–13.

[60] Jain A, Lamark T, Sjottem E, et al. p62/SQSTM1 is a target gene for transcription factor NRF2 and creates a positive feedback loop by inducing antioxidant response element-driven gene transcription. J Biol Chem. 2010;285(29):22576–22591.

[61] Panek J, Kolar M, Vohradsky J, et al. An evolutionary conserved pattern of 18S rRNA sequence complementarity to mRNA 5′ 5′ UTRs and its implications for eukaryotic gene translation regulation. Nucleic Acids Res. 2013;41(16):7625–7634.

[62] Pankiv S, Clausen TH, Lamark T, et al. p62/SQSTM1 binds directly to Atg8/LC3 to facilitate degradation of ubiquitinated protein aggregates by autophagy. J Biol Chem. 2007;282(33):24131–24145.

[63] Menzies FM, Rubinsztein DC. Broadening the therapeutic scope for rapamycin treatment. Autophagy. 2010;6(2):286–287.

[64] Quarles E, Basisty N, Chiao YA, et al. Rapamycin persistently improves cardiac function in aged, male and female mice, even following cessation of treatment. Aging Cell. 2020;19(2):e13086.

[65] Sarkar S, Krishna G, Imarisio S, et al. A rational mechanism for combination treatment of Huntington's disease using lithium and rapamycin. Hum Mol Genet. 2008;17(2):170–178.

[66] Zhang N, Li B, Al-Ramahi I, et al. Inhibition of lipid signaling enzyme diacylglycerol kinase epsilon attenuates mutant huntingtin toxicity. J Biol Chem. 2012;28717(25):13170–13178.

[67] Giustiniani J, Sineus M, Sardin E, et al. Decrease of the immunophilin FKBP52 accumulation in human brains of Alzheimer's disease and FTDP-17. J Alzheimers Dis. 2012;29:471–483.

[68] Avramut M, Achim CL. Immunophilins and their ligands: insights into survival and growth of human neurons. Physiol Behav. 2002;77(4–5):463–468.

[69] Caraveo G, Soste M, Cappelleti V, et al. FKBP12 contributes to alpha-synuclein toxicity by regulating the calcineurin-dependent phosphoproteome. Proc Natl Acad Sci U S A. 2017;114(52): E11313–e22.

[70] Caron NS, Desmond CR, Xia J, et al. Polyglutamine domain flexibility mediates the proximity between flanking sequences in huntingtin. Proc Natl Acad Sci U S A. 2013;110 (36):14610–14615.

[71] Neveklovska M, Clabough EB, Steffan JS, et al. Deletion of the huntingtin proline-rich region does not significantly affect normal huntingtin function in mice. J Huntington's Dis. 2012;1 (1):71–87.

[72] Sun CS, Lee CC, Li YN, et al. Conformational switch of polyglutamine-expanded huntingtin into benign aggregates leads to neuroprotective effect. Sci Rep. 2015;5(1):14992.

[73] Martin DD, Ladha S, Ehrnhoefer DE, et al. Autophagy in Huntington disease and huntingtin in autophagy. Trends Neurosci. 2015;38(1):26–35.

[74] Guo F, Liu X, Cai H, et al. Autophagy in neurodegenerative diseases: pathogenesis and therapy. Brain Pathol. 2018;28 (1):3–13.

[75] Sarkar S, Davies JE, Huang Z, et al. Trehalose, a novel mTOR-independent autophagy enhancer, accelerates the clearance of mutant huntingtin and alpha-synuclein. J Biol Chem. 2007;282(8):5641–5652.

[76] Sarkar S, Ravikumar B, Floto RA, et al. Rapamycin and mTOR-independent autophagy inducers ameliorate toxicity of polyglutamine-expanded huntingtin and related proteinopathies. Cell Death Differ. 2009;16(1):46–56.

[77] Leavitt BR, Kordasiewicz HB, Schobel SA. Huntingtin-lowering therapies for huntington disease: a review of the evidence of potential benefits and risks. JAMA Neurol. 2020;77(6):764.

[78] Ravikumar B, Vacher C, Berger Z, et al. Inhibition of mTOR induces autophagy and reduces toxicity of polyglutamine expansions in fly and mouse models of Huntington disease. Nat Genet. 2004;36(6):585–595.

[79] Li Z, Wang C, Wang Z, et al. Allele-selective lowering of mutant HTT protein by HTT-LC3 linker compounds. Nature. 2019;575 (7781):203–209.

[80] Martinez-Vicente M, Talloczy Z, Wong E, et al. Cargo recognition failure is responsible for inefficient autophagy in Huntington's disease. Nat Neurosci. 2010;13(5):567–576.

[81] Steffan JS. Does Huntingtin play a role in selective macroautophagy? Cell Cycle. 2010;9(17):3401–3413.

[82] Gassen NC, Hartmann J, Zschocke J, et al. Association of FKBP51 with priming of autophagy pathways and mediation of antidepressant treatment response: evidence in cells, mice, and humans. PLoS Med. 2014;11(11):e1001755.

[83] Cheung-Flynn J, Prapapanich V, Cox MB, et al. Physiological role for the cochaperone FKBP52 in androgen receptor signaling. Mol Endocrinol. 2005;1936(6):1654–66585-595.

[84] Kl R, An MC, Zhang N, et al. Genomic Analysis Reveals Disruption of Striatal Neuronal Development and Therapeutic Targets in Human Huntington's Disease Neural Stem Cells. Stem Cell Reports. 2015;5(6):1023–1038.

[85] Kemp PJ, Rushton DJ, Yarova PL, et al. Improving and accelerating the differentiation and functional maturation of human stem cell-derived neurons: role of extracellular calcium and GABA. J Physiol. 2016;594(22):6583–6594.